Mapping and monitoring oilseed rape fields using Sentinel-1 time-series data

YIZHANJIAO
June, 2020

SUPERVISORS:
Dr. Tiejun Wang
Drs.Raymond Nijmeijer

Mapping and monitoring oilseed rape fields using Sentinel-1 time-series data

YIZHAN JIAO
Enschede, The Netherlands, [June, 2020]

Thesis submitted to the Faculty of Geo-Information Science and Earth Observation of the University of Twente in partial fulfilment of the requirements for the degree of Master of Science in Geo-information Science and Earth Observation.
Specialization: Natural Resources Management

SUPERVISORS:
Dr. Tiejun Wang
Drs.Raymond Nijmeijer

THESIS ASSESSMENT BOARD:
Dr. Yousif Hussin (Chair)
Dr. Zoltán Vekerdy (External Examiner, University of Twente)
etc

ABSTRACT

Rapeseed is one of the most important oilseed crops in the world, which has been used in many ways as edible oil, industrial oil, and feed. As croplands vary over space and time, accurate and updated maps of rapeseed fields are needed for studies of food security. The conventional field survey method for crop mapping is time and labor-consuming. Remotely sensed data has been proved as a credible source for crop mapping. Although optical imagery can be used to map rapeseed fields, it is highly influenced by cloud cover. This study assessed the feasibility of weather independent space-borne Synthetic Aperture Radar (SAR) Sentinel-1 data for mapping and monitoring rapeseed fields in a cloudy area of China. Backscatter coefficients (VH and VV) and decomposition features (i.e., entropy, anisotropy, angle) of Sentinel-1 time-series data were used in this study. Both Support Vector Machine and Random Forests classifiers were employed to classify rapeseed fields and their performances have been compared in terms of overall accuracy as well as kappa statistic. It was found that the highest classification accuracy was achieved by using Sentinel-1 time-series data, with overall accuracy greater than 99% and a kappa coefficient greater than 0.98 through both Random Forests and Support Vector Machine classifiers, which are significantly higher than those derived from mono-temporal Sentinel-1 data. However, it was also found that there was no statistically significant difference in classification accuracy between the use of Sentinel-1 multi-temporal data (i.e., images obtained from April and May) and Sentinel-1 time-series data. Moreover, the changing pattern and change hotspot of rapeseed fields in the Hanzhong basin between 2017 and 2019 have been successfully quantified and identified. The results from this study demonstrate that multi-temporal Sentinel-1 SAR images can be used for accurate and timely rapeseed field mapping and monitoring.

Keywords: rapeseed, Sentinel-1, random forest, support vector machine, time series, multi-temporal

ACKNOWLEDGEMENTS

This thesis is the final output of my 24 months life as a student of Geo-Information Science and Earth Observation (ITC) of the University of Twente, from where I learned a lot. Here, I would like to express my sincere appreciation to all the people who helped and supported me during the research.

Foremost, I gratefully acknowledge the guidance of my first supervisor Dr. Tiejun Wang for the continuous support of my master's study and thesis work. I learned a lot from your patience, professional, and scientific guidance. I sincerely apricate the advises that you gave me during every discussion. And also thank you very much for your concerns in this weird period. I really enjoyed your supervision.

My special appreciation to Drs. Raymond Nijmeijer, my second supervisor, for helping me in scientific writing. You are not only my second supervisor but also my course director, you made my study life easier with your wise suggestions.

Also, thanks to Dr. Yousif Hussin and the assessment board during my proposal and mid-term presentation, for constructive comments and suggestions. Moreover, I would like to thank all teachers who taught me in different courses, I benefited a lot from your professional teaching.

My appreciation for all my colleagues and friends in ITC. Thank you for your company in every class, fieldwork, discission, and parties.

Finally, my sincerest thanks to my parents for your unconditional support in both physical and spiritual to me during the MSc life here.

TABLE OF CONTENTS

LIST OF FIGURES

LIST OF TABLES

1. INTRODUCTION

1.1. Background

Oilseed rape (*Brassica napus* L.), also known as rapeseed, is a member of the family Brassicaceae (Hall et al., 2002). Rapeseed has seeds with high oil content (~40%) (Zafar et al., 2019) and because of its oil-rich property, rapeseed is now the third-largest source of vegetable oil in the world right after soybean oil and palm oil. It and accounting for 16% world's edible oil (Eskin and Przybylszi, 2003) and therefore plays an essential role in securing edible oil worldwide. Besides its edible property, rapeseed is also often used as industrial renewable oil owing to its biodegradable property (Saka & Kusdiana, 2001). The rapeseed and its derivatives are essential commodities and closely related to the lives of people in the world. Thanks to its multiple uses, rapeseed is cultivated all over the world. Based on the statistics from the Food and Agricultural Organization of the United Nations (FAO), the global cultivated area of rapeseed has increased dramatically since the mid-twentieth century till the beginning of the twenty-first century (FAO, 2019). Leading producers in rapeseed production are China, Canada, and the EU (Woz´niak et al., 2019).

However, global rapeseed production has declined in recent years. According to FAO statistics, the area under rapeseed cultivation around the world was 34,377,958 hectares. That is 1,869,605 hectares less than that in 2015, which is almost a decrease of 6% (FAO, 2019). The cultivated area of rapeseed has declined by 8.3% in the EU in 2019 (Krautgartner et al., 2019). An up to date crop map generated by the Center for Ecology & Hydrology (CEH) and RSAC Ltd shows an overall 15% decrease in fields of rapeseed planted across Britain in the last 3 years (CEH, 2017).

Turning the perspective to China which is the biggest producer of oilseed rape and accounting for 20% of total rapeseed approximately, the planted area of rapeseed remains stable in recent years (Hu et al., 2017). However, the interest of rapeseed farmers in China is declining as the years go by due to increased labor and input costs (Fu, 2016). Also, under the trend of a sharp decline in international acreage, the cultivated area of rapeseed in China is particularly important and needs to be maintained in supporting the sufficient supply of rapeseed. Therefore, to help the decision making in meeting the yield consumption, the distribution of rapeseed in China urgently needs to be mapped accurately in both spatial and temporal dimensions (Liu et al., 2018).

Agricultural mapping plays an essential role in monitoring as well as the management of land cropping (Vaudour et al., 2010). For instance, agricultural mapping can be used in yield estimation (Awad., 2019) and the evaluation of the provision of ecosystem services (Koschke et al., 2013). field surveying is the conventional method in monitoring and mapping crops. However, despite the high accuracy provided by the field survey, the limitations are time-consuming, expensive, labor-intensive, and hard to be applied to a large area (Huang et al., 2012).

1.2. Remote Sensing of Crops

The use of remote sensing data in agricultural mapping started in the 1970s. Compared to field survey methods, using remote sensing data to map crops can be applied at a larger scale with a lower cost. Consequently, remote sensing has been widely used in agricultural classification (Atzberger, 2013). Commonly, remotely sensed mapping and monitoring of crops could be divided into two classes: the optical remote sensing and radar technology. Optical remote sensing has many applications in crop mapping such as rice (Dong & Xiao, 2016; Song et al., 2018; Zhang & Lin, 2019) and wheat (Nagy et al., 2018; Tao et al., 2017; Sánchez et al., 2014). Vaudour et al. (2015) used very high-resolution Pleiades images in the early season to map rapeseed fields and get 87% classification accuracy. Wang et, al (2018) produced a regional distribution map of rapeseed fields in China and achieved 85% overall accuracy. But in these studies, due to the big overlap between the rapeseed growing season and the rainy season, the cloud-cover problem exists and highly influences the optical imagery(Myneni et al., 1995).

Radar technology is a good alternative in mapping and monitoring crops. Compared to optical remote sensing, the microwave wavelengths used by radar can stride through clouds. An active remote sensing technology like the Synthetic Aperture Radar (SAR) can acquire data during the night (Richards, 2015). Besides, Stankiewicz (2006) demonstrated that backscattered radar signals of the agricultural fields are determined by soil conditions, surface roughness, biomass structure, and water content in both soil and leaves. Furthermore, Choudhury and Chakraborty (2006) concluded that the different backscattered signals of cropland could be regarded as a function of growth time.

Many studies demonstrated the relevance of SAR data for crop monitoring (Aschbacher et al., 1995; Jiao et al., 2014; Wu et al., 2011). In terms of rapeseed, several studies have shown the value of SAR data for identifying rapeseed growth stages. Lampropoulos et al., (2015) demonstrated that rapeseed growth stages could be detected by SAR polarimetric parameters such as scattering diversity and polarization methods. In light of this discovery, the phenology of rapeseed in Canada has been estimated successfully (McNairn et al., 2018). These applications showed the potential of SAR technology in rapeseed mapping.

SAR sensors can vary in bands and polarization methods. Radar polarization is the orientation of the electric field. The transmitted and received signal can be either horizontally (H) or vertically (V) polarized (ESA, 2015). Thus, four possible combinations of orientations of transmitted and received exist HH, VV, VH, and HV. In crop mapping, single-polarization (VV) can be used in detecting vertical changes such as vegetation height with the crop growing (McNairn & Brisco, 2004). Cookmartin et al. (2000) demonstrated that Sigma VV is sensitive to vegetation wetness. The cross-polarization is robust in distinguishing the scattering mechanism in the canopy (Cloude, 2007). However, (Ferrazzoli et al., 2013) pointed out the shortages of using single-polarization methods and single orbit-pass, and that the use of dual-polarization leads to a significant increase in the final classification accuracy. Therefore, studies used dual-polarization SAR data for wetland vegetation mapping (Fu et al., 2017), vegetable classification (Li & Bijker, 2019), polluted vegetation mapping, and so on. The selection of the band needs to adapt to the surface targets, and which parts of the target interact with SAR signals need to be considered (Cloutis, 1999; McNairn & Brisco, 2004). As shown in Figure 1, the band with shorter wavelengths such as X-band reflects at the top of the canopy while the longer wavelength C-band interacts with the canopy and the bands with the longest wavelengths such as P-band and L-band can go across the canopy. Most of the studies focused on detecting crops using X-band and C-band sensors to get the backscattered signals less influenced by the underlying soils (Wang et al., 2019). The capability of C-band in detecting backscattered signals from crops as well as crop classification has been proved (McNairn et al. , 2009; Cai et al., 2019).

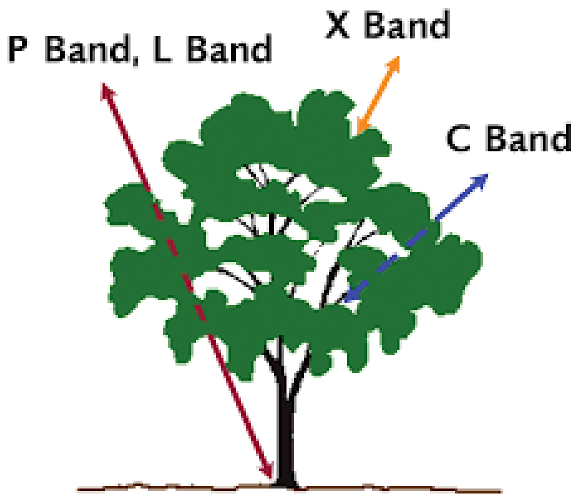

Figure 1: The interaction between canopy and signals with different wavelengths.

(source: http://www.intelligenceairbusds.com/files/pmedia/edited/r15796_9_eij_radarimagery_finalarticle.pdf)

SAR decomposition can also provide information related to the contributions of different scattering mechanisms (Cloude et al., 1996). In terms of vegetation canopies, scattering mechanisms are related to the biomass and vegetation structure (Mcnairn et al., 2009). Fang et al. (2018) used GF-3 polarimetric SAR data to classify 7 land-cover classes and was able to obtain an 83.20% overall accuracy. Denize et al. (2019) achieved 71.7% overall accuracy in winter land-use classification by using Sentinel-1 polarimetric SAR data. Therefore, in this study, the combined use of backscatter coefficients and polarimetric information in rapeseed mapping was assessed.

Considering the seasonal variation in backscatter SAR signals caused by changes in biomass structure and the water content in both soil and leaves with vegetation growth, increasing numbers of vegetation classification applications used multi-temporal or time-series images instead of mono-temporal data (Stendardi et al., 2019). Kavats et al. (2019) pointed out using time-series SAR data helps to improve the separability of crop types compared with using mono-temporal SAR data. Applications using multi-temporal SAR images in urban, forest, and agriculture land cover classification can be easily found (Le Toan et al., 1989; Pellizzeri et al., 2003). Besides, Wu et al. (2011) used three RADARSAT-2 images obtained before and after rice harvesting and get 88.91% overall accuracy in rice classification. Similarly, Hütt et al. (2017) used five TerraSAR-X images in crop classification and achieved nearly 90% overall accuracy. Sharp changes in terms of vegetation structure between growth stages (i.e. before and after harvesting) were captured by the SAR sensor, therefore, high classification accuracy was achieved (Veloso et al, 2017).

1.3. Problem Statement

As an important rapeseed cultivation country, Chinas rapeseed planted area, and its changes are strongly related to the supply of edible oil globally. Thus, the rapeseed distribution in China needs to be mapped accurately. Especially in areas such as the Hanzhong basin which is one of the most important rapeseed production areas and a scenic famous for its vast "rapeseed flowers sea". However, in such an essential rapeseed cultivated area, the understanding of rapeseed planted area and its changes spatially and temporally was limited due to the lack of rapeseed distribution maps in China on a regional scale (Wang et al., 2018).

Time-series SAR data can identify different land-cover types by comparing the temporal performance of backscatter coefficients (Bruzzone et al., 2004) and therefore improve the ability to distinguish land-cover classes. It is hard to use a mono-temporal image in the crop classification due to the similarity in backscatter coefficients which is caused by the resemblance in scattering mechanism, vegetation structure, etc. between different land-cover classes. Besides, the results of some studies showed a high classification accuracy when using multi-temporal data of some certain growth stages of vegetation. Thus, it is worth exploring the optimal multi-temporal combination of rapeseed mapping.

C-band SAR data has been widely used in vegetation mapping. Sentinel-1 data has great potential for rapeseed mapping thanks to its improvements in terms of temporal resolution and spatial coverage (ESA, 2013). Many studies used Sentinel-1 images in analyzing rapeseed in terms of phenological stages (Mercier et al., 2020; d'Andrimont et al., 2020), and studies that used the combination of Sentinel-1 images with optical data in rapeseed classification can be found as well (Lussem et al., 2016). However, only a few studies mapping rapeseed use only Sentinel-1 SAR data. Therefore, it is worth further exploring the use of Sentinel-1 images to map rapeseed fields in the Hanzhong basin.

1.4. Research Objectives

The overall objective of this study is to map and monitor rapeseed fields in the Hanzhong basin in China using Sentinel-1 SAR data. The specific objectives of this research are as follows:

1. To understand how the Sentinel-1 radar signals respond to the growth of rapeseed.

2. To determine the optimal timing for mapping rapeseed fields using mono-temporal, multiple temporal, and time-series Sentinel-1 images.

3. To compare the rapeseed field mapping accuracy between the use of the random forest classifier and the support vector machine classifier.

4. To quantify the change of the rapeseed fields in the Hanzhong basin in China between 2017 and 2019.

1.5. Research questions

1. How do the Sentinel-1 radar signals respond to the growth of rapeseed?

2. What is the optimal timing for mapping rapeseed fields using Sentinel-1 data?

3. Is there a significant difference in rapeseed field mapping accuracy between the use of the random forest model and the support vector machine model using Sentinel-1 data?

4. How do the rapeseed fields change in the Hanzhong basin in China between 2017 and 2019？

1.6. Research hypothesis

1)
H0: There is no statistically significant difference in rapeseed mapping accuracy between the use of single date, multiple dates, and time-series Sentinel-1 data.

H1: The rapeseed mapping accuracy in using time series is significantly higher than that using a Mono-temporal date and multi-temporal data.

2)
H0: There is no significant difference in rapeseed mapping accuracy between the use of the random forest model and the support vector machine model.

H1: The rapeseed mapping accuracy derived from the random forest model is significantly higher than the one derived from the support vector machine model.

3)
H0: There is no significant change in the area of rapeseed fields in the Hanzhong basin between 2017 and 2019.

H1: The area of the rapeseed fields has been changed significantly in the Hanzhong basin between 2017 and 2019.

2. MATERIALS AND METHODS

2.1. Study Area

The Hanzhong basin is located in between Qinling Mountain and Daba Mountain (32°08'54" N~33°53'16"N, 105°30'50"E~108°16'45"E) and belongs to Shaanxi province, China. The Hanzhong basin lies a typical north subtropical monsoon climate zone. The prevailing climate of this basin is temperate and humid, with an average temperature of 14.33°C and 853 mm precipitation annually (Xiao et al., 2019). The terrain of the Hanzhong basin is gradually decreasing from north to the south. The forest coverage rate reached 52% with a high species diversity thanks to the excellent ecological environment. By 2017, the population in the basin was 3.44 million, the GDP 133 billion, the total crops cultivated area was more than 2000 km2, and the agricultural production per year was 1 million tons (Sun et al., 2020). Thus, the Hanzhong basin is called the "land of Fish and Rice" and "land of abundance".

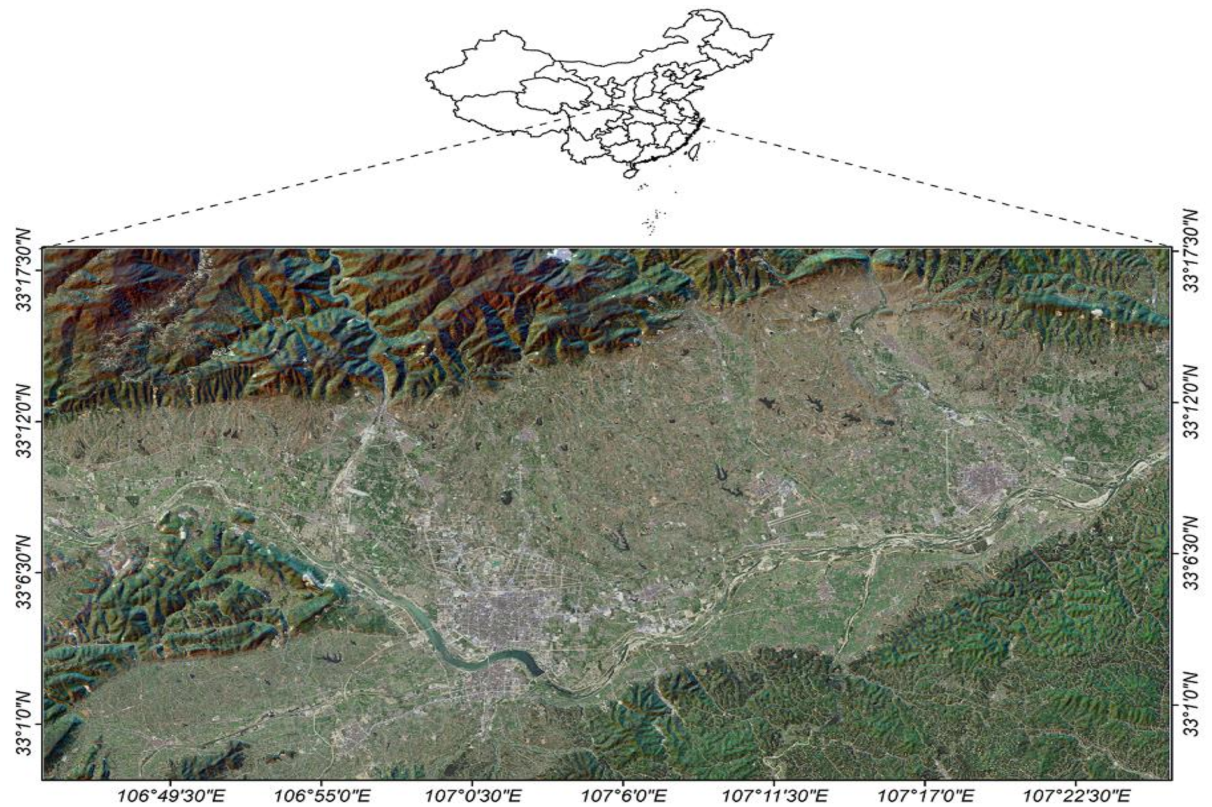

Figure 2 The location of the study area in China (display in RGB band)

In China, rapeseeds are mainly planted in areas near the Yangtze River (Zhang & He, 2013). Han River is the biggest river in the Hanzhong basin as well as the largest tributary of the Yangtze River (Xiao et al., 2019). Thanks to the unique geographical advantages of the Hanzhong basin and the strong support of the local government, rapeseeds have been vastly planted in the Hanzhong basin. The "rape flower sea" is attracting tourists from all over the world and is regarded as a huge support for the local tourism industry. Also, benefit by the relatively flat terrain of the Hanzhong basin, the Radar distortions such as radar shadow and foreshortening in radar images caused by rugged terrains will barely happen. Therefore, it is very representative to choose the Hanzhong basin as the study area using Sentinel-1 images to map and monitor rapeseed fields and have a basic understanding of rapeseed in China.

2.2. Data

2.2.1. Sentinel-1 Image And Pre-processing

The Sentinel-1 mission, as a European Radar Observatory of Copernicus, was co-promoted by the European Commission and the European Space Agency (ESA). It is contained by two constellation satellites: Sentinel-1A and Sentinel-1B. Sentinel-1A was launched in April 2014 while Sentinel-1B was launched in April 2016. As a SAR C-band sensor, Sentinel-1 provides free accessible data with four possible polarizations: single-polarization (VV, VH) and dual-polarization (VV+VH, HH+HV). The data is acquired in four modes, i.e., SM (StripMap), IW (Interferometric Wide swath), EW (Extra-Wide swath), WV (Wave). Sentinel-1 data has three-levels: level-0 raw data, level-1 geo-referenced time-tagged data (Single look Complex, Grand Range Detected), and level-2 ocean-use data with 12 days temporal resolution (ESA, 2013). The metadata of collected Sentinel-1 IW images is shown in Table 1.

Table 1 Overview of Sentinel-1 data

Parameter	Interferometric Wide swath
Polarization	Dual VV+ VH
Azimuth Resolution	<20 m
Ground Range resolution	<5 m
Azimuth and range look	Single
Swath	>250 km
Maximum NESZ	-22dB
Radiometric stability	0.5 dB
Radiometric Accuracy	1 dB
Phase Error	5^0
Acquisition Date	2018. 10. 7/ 2018. 10. 19/ 2018. 10. 31/ 2018. 11. 12/ 2018. 11. 24/ 2018. 12. 06/ 2018. 12. 18/ 2018. 12. 30/ 2019. 01. 11/ 2019. 01. 23/ 2019. 02. 04/ 2019. 02. 16/ 2019. 02. 28/ 2019. 03. 12/ 2019. 03. 24/ 2019. 04. 05/ 2019. 04. 17/ 2019. 04. 29/ 2019. 05. 11/ 2019. 05. 23/ 2019. 06. 04/ 2017. 04. 03/ 2017. 04. 15/ 2017. 04. 27/ 2017. 05. 09/ 2017. 05. 21/

Table 1

In this study, the standard level 1 product of Single Look Complex (SLC) collected in IW mode and polarized in VH and VV was selected. As shown in Table 1, to map rapeseed fields in 2019, 21 images collected from October 7th of 2018 to June 5th of 2019 were selected. As for mapping rapeseed fields in 2017, 5 images collected from April 1st of 2017 to May 28th of 2017 were selected. By using the Sentinel Application Platform (SNAP) Toolbox developed by ESA, images can be converted from digital number(DN) values to selected variables. In addition to Sigma VH and Sigma VV, two backscatter indices were calculated, namely Sigma VV – Sigma VH, and normalized difference polarization index (NDPI) (Cao et al., 2018). The potential of two backscatter indices in vegetation classification has been proved (Li and Bijker, 2019). The calculation of NDPI is:

$$\frac{\sigma_{vv} - \sigma_{vh}}{\sigma_{vv} + \sigma_{vh}}$$

In this study, two pre-processing methods were used. To get Sigma VH, Sigma VV, VV-VH, and NDPI, the specific processing steps are as follows:

1) Apply orbit file. In SAR source products, the orbit information is generally inaccurate. Thus, the accurate orbit information auto-downloaded by SNAP needs to be applied.

2) Split. The Sentinel-1 IW images were stored in split sub-swath. This step helps to zoom into the study area by selecting the sub-swath of interests.

3) Thermal noise removal. SAR products are highly influenced by thermal noise, especially in the cross-polarization channel. The thermal noise removal step helps to reduce thermal noise.

4) Calibration. RADAR calibration is a process that transfers the digital pixel values to calibrated SAR backscattered singles. In this step, backscatter singles are saved in Sigma format.

5) De-burst. The purpose of this step is to remove the gaps between each selected sub-swath.

6) Speckle filter. In SAR images, speckles refer to granular noise caused by interference of waves that are reflected from all kinds of elementary scatters. The speckle filter was applied to the SAR images to decrease influences caused by speckles and enhance the quality of images. The Refined Lee filter with a 3 by 3 window size was used in this study owing to its capability in speckle removing while the edge information reserves.

7) Terrain correction. In SAR images, geometry distortions caused by side-looking occur frequently. The Range Doppler Terrain correction method with SRTM 3ec DEM was applied to the SAR images and the images were reprojected to the Universal Traverse Mercator coordinate system (UTM zone 48N, WGS 84).

8) From linear to dB. The source backscatter coefficients were stored in unitless values and converted to dB using a logarithmic transformation.

9) Band math. After eight pre-processing steps above, Sigma VH and Sigma VV can be obtained and the values of VV-VH and NDPI can be calculated through band math.

In addition to backscatter coefficients, features (entropy, alpha, and anisotropy) derived from Sentinel-1 SAR data through SAR H-Alpha Dual-Polarization decomposition were used. H-Alpha Dual-Polarization is modified for dual-polarized data (Cloude and Pottier, 1997). Entropy-Alpha plane is commonly used in representing the relation between decomposition features and scattering mechanisms through a nine-zone segmentation (Table2) (Yonezawa et al., 2012).

Table 2 The entropy-alpha plane partitioned into nine zones.

Zone	Entropy	Alpha	Scattering type
1	0.9-1	55–90	High Entropy Multiple Scattering
2	0.9-1	40–55	High Entropy Vegetation Scattering
3	0.9-1	0-40	High Entropy Surface Scattering
4	0.5-0.9	50-90	Medium Entropy Multiple Scattering
5	0.5-0.9	40-50	Medium Entropy Vegetation Scattering
6	0.5-0.9	0-40	Medium Entropy Surface Scattering
7	0-0.5	47.5-90	Low Entropy Multiple Scattering
8	0-0.5	42.5-47.5	Low Entropy Dipole Scattering
9	0-0.5	0-42.5	Low Entropy Surface Scattering

To get entropy, anisotropy, and alpha, the specific pre-processing steps are as follows (note that repeated pre-processing steps are not explained in detail): 1) Apply orbit file. 2) Split. 3) Calibration. In this step, backscatter singles are saved in complex output. 4) De-burst. 5) Polarimetric Matrix generation. To generate the scattering matrix backscatter singles are stored in complex numbers and the polarimetric matrix needs to be applied using the default c2 method through SNAP. 6) Speckle filter. 7) Terrain correction. 8) Polarimetric decomposition. To obtain entropy, anisotropy, and alpha, the polarimetric decomposition needs to be applied in the H-Alpha Dual-Pol decomposition method through in SNAP. After that, all chosen bands are resampled to 20-meter spatial resolution using the nearest neighbor method. Figure 3 shows the pre-processed Sentinel-1 data obtained on April 29th, 2019.

F

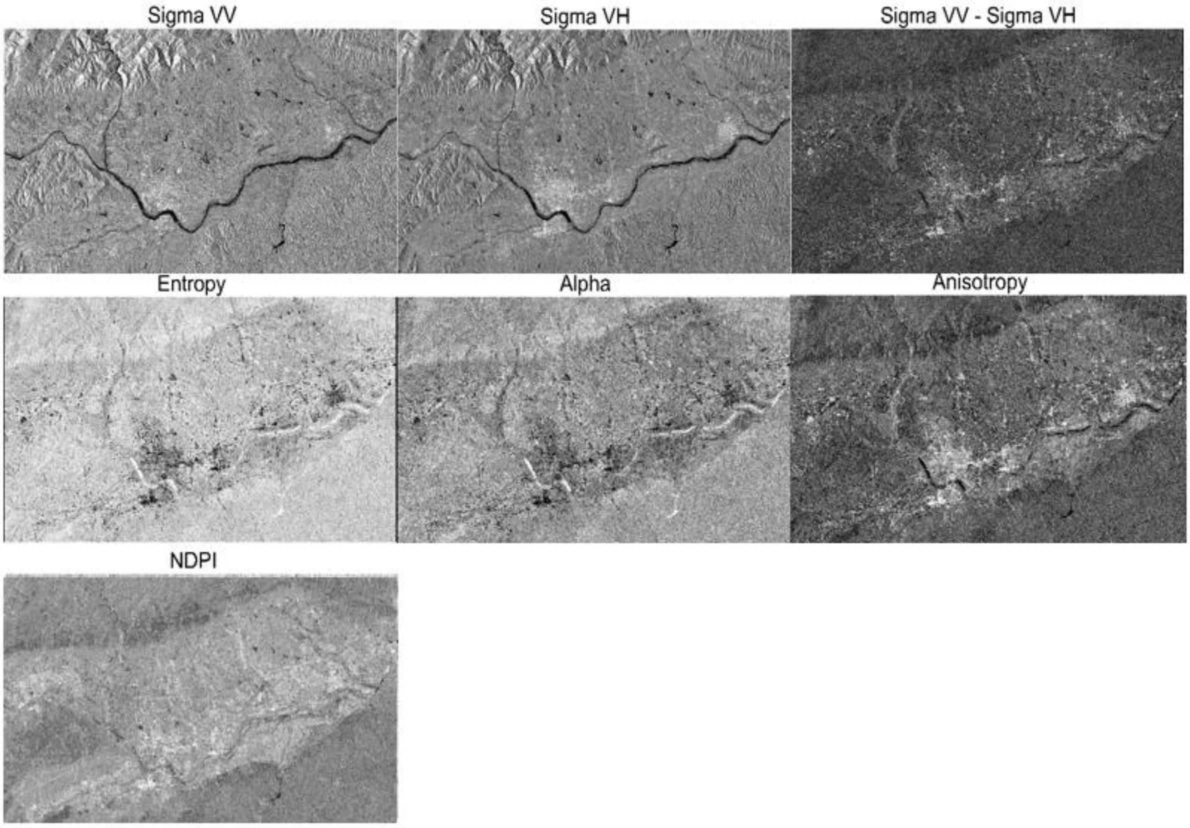

Figure 3 Features derived from Sentinel-1 data (April 29th of 2019).

2.2.2. Topographic Data

In this study, topographic information including DEM, aspect, and the slope was extracted from 30m SRTM Digital Elevation Model (DEM) Version 2 released by the ministry of economy, trade, and industry (METI) and the United States national aeronautics and space administration (NASA) on October 17th of 2011. The DEM data were geometrically co-registered with Sentinel-1 images using nearest-neighbor interpolation. The topographic modeling tool provided by ENVI software (version 5.3) has been used in extracting aspect and slope.

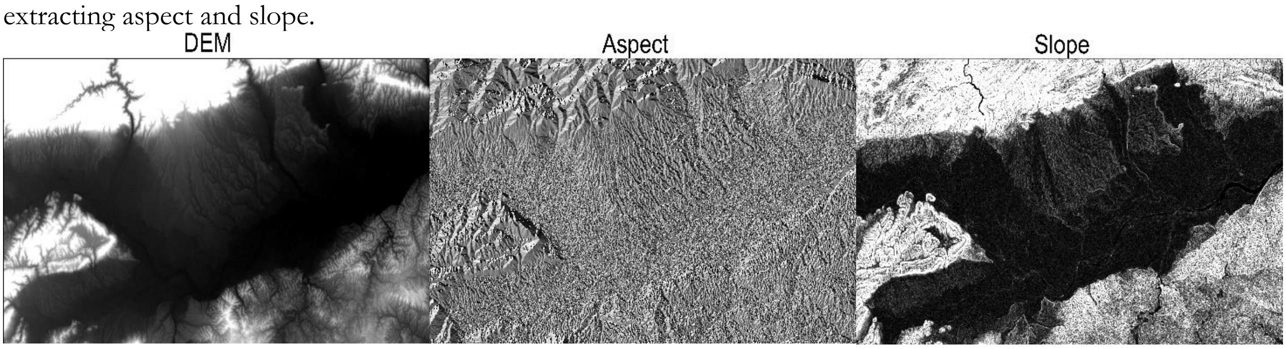

Figure 4 Features derived from DEM data.

2.2.3. Field Data

The sampling method used in this study is stratified random sampling. Compare to normal random sampling, stratified random sampling highlights the differences between strata, rather than treat all population as equal. Two strata were defined a) rapeseed fields and b) non-rapeseed. In the non-rapeseed strata, 5 land cover types were selected 1) Waterbody 2) Forest 3) Wheatfields 4) Build-up area 5) Bare soil, and 6) Vegetable (Sun et al., 2014). The rapeseed fields data for training and validation in the Hanzhong basin in 2019 were obtained from the field. Fieldwork was conducted in August 2019, which is not a local rapeseed growing season. However, with the help of local experts and high-resolution RapidEye images obtained in the rapeseed growing season（April 14th 2019), fields in which rapeseed was planted last season can still be distinguished. Central points of rapeseed fields that reached a size of 50m*50m were collected as sample points and GPS positions of these central points were obtained. The GPS position of non-rapeseed points was collected using the same method. In total there are 180 rapeseed sample points and 180 non-rapeseed sample points collected. 2/3 of rapeseed and non-rapeseed ground truth data was randomly selected for training, and the remaining 1/3 of ground truth data was used for validation.

The ground truth data for training and validation in the Hanzhong basin in 2017 was based on visual interpretation of a high-resolution RapidEye image （11 April 2017. Similarly, 180 rapeseed sample points and 180 non-rapeseed sample points were selected and 2/3 of rapeseed and non-rapeseed ground truth data were used for training while 1/3 of rapeseed and non-rapeseed ground truth data were used for validation. Figure5 and Figure6 show the distribution of selected training and validation points of 2017 and 2019 respectively. Besides, to reduce the inconsistency in sample selection between 2017 and 2019 and to make the classification accuracy of 2017 and 2019 comparable, an extra 60 rapeseed fields sample points and 60 non-rapeseed sample points that have no change between 2017 and 2019 were selected through visual interpretation, and, all these 120 sample points were be used for validation (Shown in Figure7).

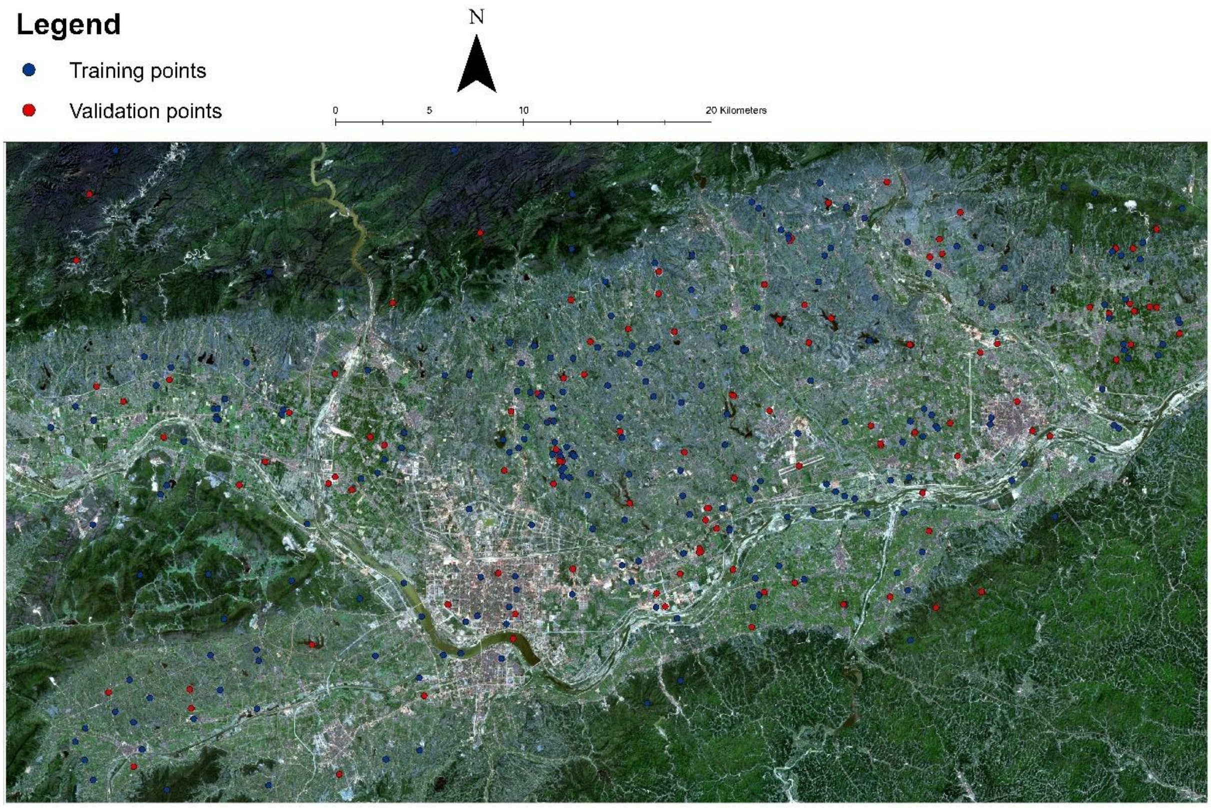

Figure 5 Training and sampling points used for rapeseed mapping in the Hanzhong basin in 2017

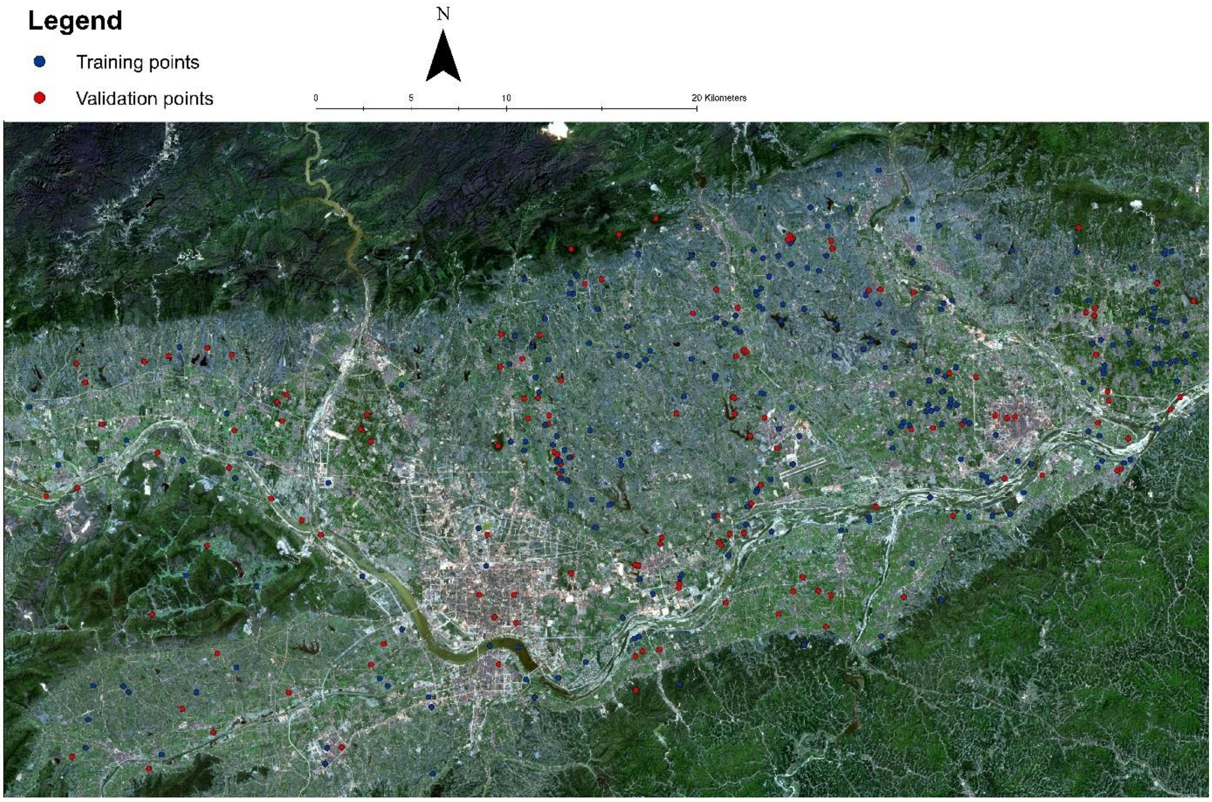

Figure 6 Training and sampling points used for rapeseed mapping in the Hanzhong basin in 2019

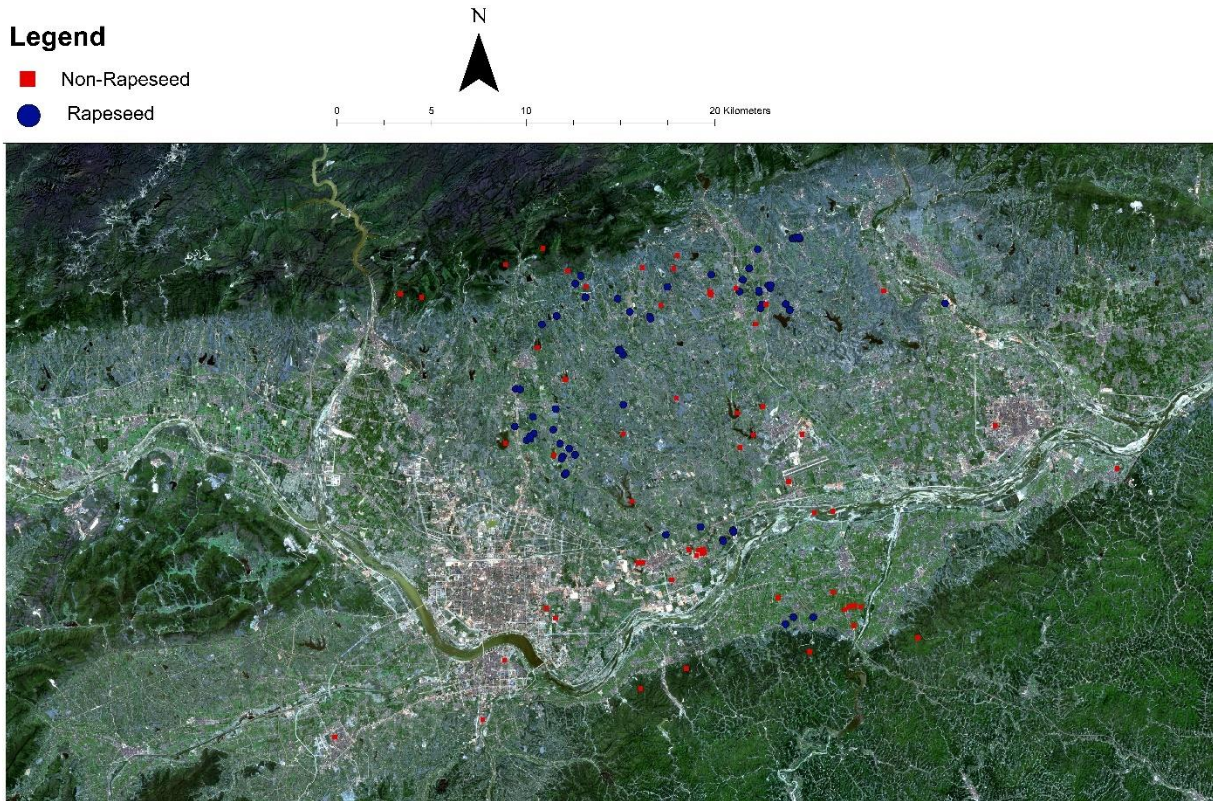

Figure 7 Additional 120 sample points of rapeseed and non-rapeseed in the Hanzhong basin

2.2.4. Crop calendar for rapeseed

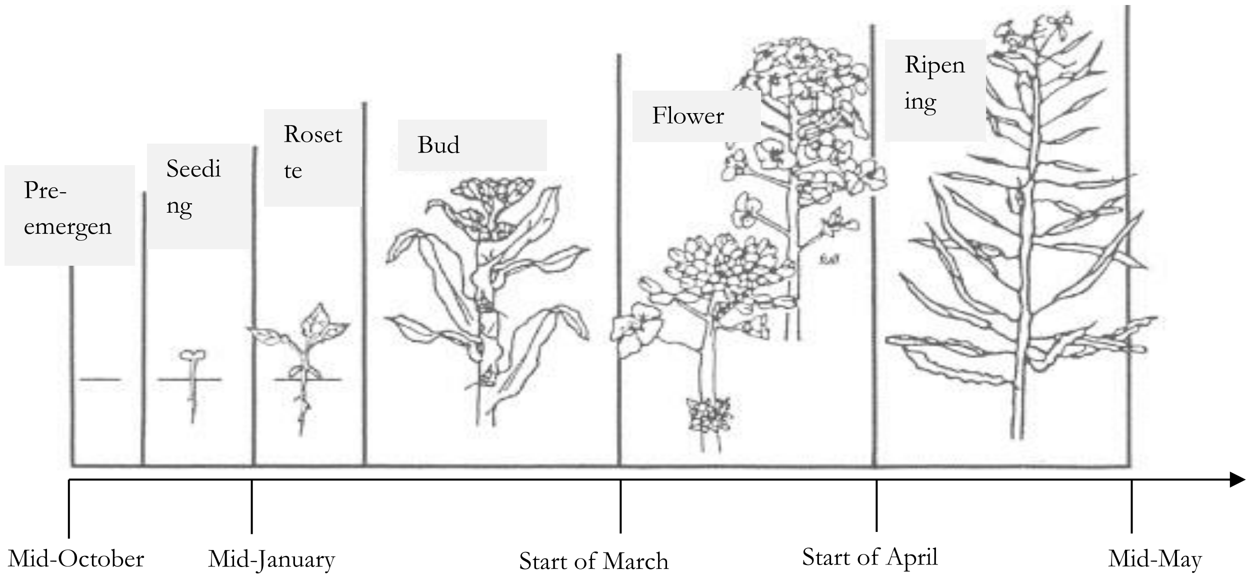

Figure 8Growth stages in rapeseed and local crop calendar of rapseed (Source: https://www.canolacouncil.org/canola-encyclopedia/crop-development/growth-stages/)

The local crop calendar of rapeseed was acquired from local experts and rapeseed planters. According to the calendar, the planting period of rapeseeds in the Hanzhong basin is from mid-October of the first year to the mid-May of the second year. The specific periods of different growth stages are 1) Pre-emergence stage and seeding stage: From mid-October to mid-January 2) Rosette stage and bud stage: From mid-January to start of March 3) Flower stage: From the start of March to mid-April 4) Ripening stage: From mid-April to mid-May.

The scattering mechanism between the radar signals and the rape field can be generated in three ways: 1) volume scattering, 2) double-bounce scattering, and 3) surface scattering. Volume scattering occurs when SAR signals interact with the rapeseed canopy, double-bounce scattering is present when SAR signals are backscattered by the boundary of the field while surface scattering happens when signals go through the canopy and are backscattered by the soil (Ustuner & Sanli, 2019).

The growth stages of rapeseed can be combined with the scattering mechanism. At the pre-emergence and seeding stage (figure 4, stages 1 and 2), the rapeseed can hardly be distinguished, and the field behaves similarly to bare soil, and therefore the dominant scattering method is surface scattering. At the rosette and bud stage (figure 4, stages 3 and 4), with the rapeseed growth, leaves and stems begin to appear, volume scattering happens and is mixed with the surface scattering. Also, some slight double-bounce scattering occurs in this stage. At the flower and ripening stage (figure 4, stages 5 and 6), the height of rapeseed reaches its peak. The dominant scattering is volume scattering, surface scattering barely happens. After harvesting, all the rapeseed is removed, and surface scattering becomes dominant again.

2.3. Classification methods

In this study, the land cover of the Hanzhong basin was classified into two classes (rapeseed and non-rapeseed) using the Random Forest classifier and Support Vector Machine classifier based on Sentinel-1 time-series data and topographic data. Ground truth data used for training and validation was obtained from the Hanzhong basin. The main process of this study can be divided into five parts: Random forest classification, Support vector machine classification, Parameter tuning, accuracy assessment, and comparison.

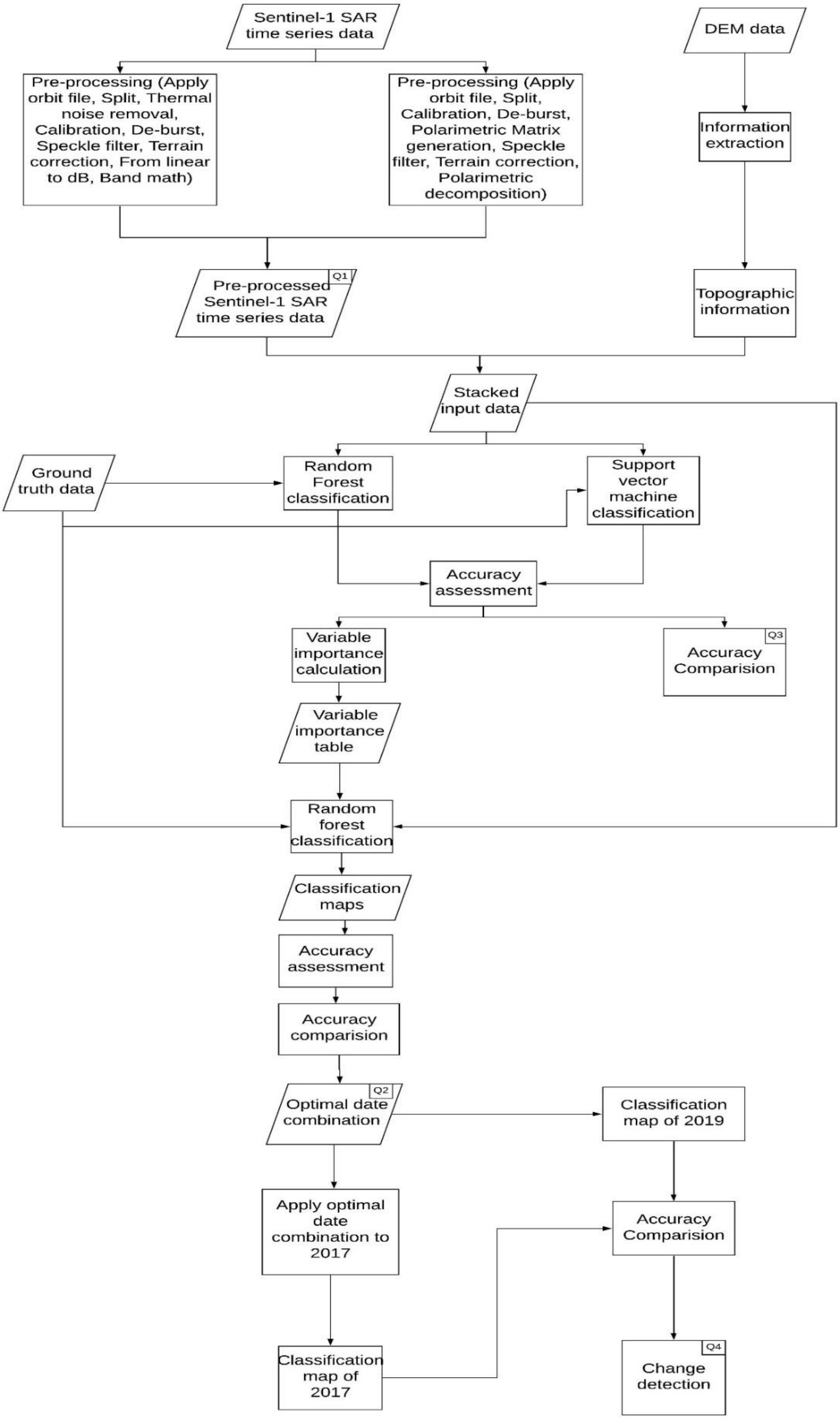

Figure 9 Flowchart of research methodology

2.3.1. Random forest algorithm

Random forest (RF) classifier is a popular and efficient ensemble supervised classification approach and has been widely used in remote sensing classification (Lu & Weng, 2007). The RF classifier equipped three main advantages. Firstly, the random forest is a non-parametric model. Compared to the parametric classification model such as Maximum likelihood, the RF classifier can operate with non-parameter distributed data, and data obtained from different remote sensing sensors can be incorporated (Belgiu & Drăguţ, 2016). Secondly, high classification accuracy can usually be provided by random forest classifier compared to other machine learning classifiers (Shang & Chisholm, 2014). Also, variable importance can be provided by random forest classifier (Chan et al., 2012). Besides, random forest classifier can deal with small sample size and is comparatively less influenced by noise (Chan & Paelinckx, 2008a). Owing to these advantages, RF classifier has been widely used in analyzing crop phenology (Wang et al., 2019), crop classification (Li et al., 2020; Tatsumi et al., 2015), and land cover mapping (Haas & Ban, 2014； Colditz & Roland, 2015). However, despite all the above-mentioned advantages of the RF classifier, the computation complexity and the long training period are always regarded as disadvantages (Zhou et al., 2020).

The random forest classifier is an ensemble of decision trees (Zhou et al., 2020). Each of these decision trees was established based on a bootstrapped sample of the training set and hold certain discriminative criteria. After trees grow, each tree will split based on user-defined reduced numbers of input variables (mtry). And, each tree will vote for the best input variable using bootstrapped samples, then the final result will be provided based on the majority of votes (Ho, 1998). In each tree, one-third of samples were selected as in-bag- samples that are used for training while the rest were selected as out-of-bag samples which are used for internal cross-validation to estimate model accuracy through out-of-bag error (Millard & Richardson, 2013).

2.3.2. Support vector machine algorithm

The support vector machine (SVM) is a classification method trying to solve classification problems by building a hyperplane. The hyperplane is based on input features from different classes and then based on the hyperplane, the unlabelled points assigned to classes (Evgeniou and pontil, 2014). The SVM classifier has its advantages in working with a small sample size, solving the problem caused by data that cannot be linearly separated and is working with high dimensional data. The SVM classifier was proposed in the late 70s and has been wildly used in solving all kinds of classification problems in the last decade. The application of the SVM classifier in crop classification such as rice, wheat, maize, and so on can be easily found. On the contrary, the difficulty in hyperparameters tuning and long training time consumed in terms of a large dataset are disadvantages of the SVM classifier.

In this study, the routine procedure of the SVM classifier contains 2 steps. Firstly, build a hyperplane that can separate input data based on kernel function, cost value, and gamma value. And secondly, based on the hyperplane to classify the pixels of input data.

2.3.3. Parameter tuning

In this study, the input predictive variables used by the RF classifier and the SVM classifier are retrieved from Sentinel-1 images and topographic data. Both the RF model and SVM model were applied in R statistical software. The specific predictive variables are Sigma VH, Sigma VV, VV-VH, NDPI, slope, aspect, elevation, entropy, anisotropy, and alpha. To implement these two classifications in R software, the dplyr package, e1071 package, caret package, and raster package were installed and used. In the RF classifier, there are two uncertain parameters, the number of decision trees (ntree) and the number of split variables in each node (mtry). The ntree was set using the default value 500 and mtry was set to 57 based on the out-of-bag error. In the SVM classifier, three essential parameters need to be defined: the kernel function, cost value, and gamma value. The default radial kernel was selected in this study, while the cost value and gamma value needed to be further determined.

The K-fold cross-validation was proposed to determine the cost value (SVM) and gamma value (SVM). Cross-validation is a popular validation method in model selection as well as parameter tuning. The routine procedure of k-fold cross-validation contains 3 steps: Firstly, split training data into k equal parts. Secondly, run the model under a particular parameter value; in this model, the first will be fold used for training while the remaining portion will be used for accuracy testing. Then the second fold will be used for training while the remaining part will be used for accuracy testing. Likewise, all folds will be used for training (shown in Figure 10). Finally, previous steps are repeated for all possible parameter values, and the most appropriate parameter can be found. Based on the parameters tuning results, the cost value was set to 5, the gamma value was set to 0.004.

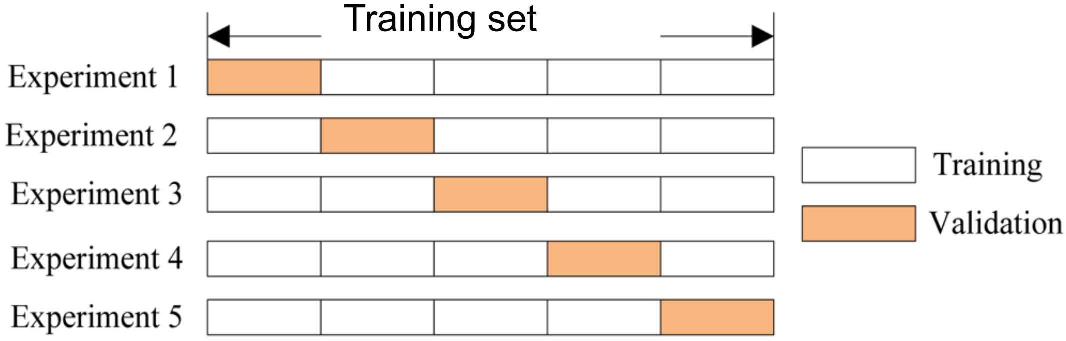

Figure 10 Illustration of K-fold cross-validation (https://scikit-learn.org/stable/modules/cross_validation.html)

2.4. Accuracy assessment

The performance of different rapeseed fields distribution maps from RF classifier or SVM classifier using either single data, multi-temporal or time-series images will be evaluated based on overall accuracy and the kappa coefficient. The overall accuracy is the most direct way to evaluate classification accuracy. However, in this study, there are only two classes (rapeseed fields, non-rapeseed) and problems of chance agreement in overall accuracy may occur. Thus, it is not rigorous to only use overall accuracy in accuracy evaluation.

To overcome the limitation of chance agreement in overall accuracy, the chance-corrected measure Cohen's kappa coefficient (Cohen, 1960) was used in this study. Cohen's kappa can measure the agreement between classified land cover classes and true land cover classes while avoiding the chance agreement, therefore regarded as a more rigorous way of accuracy assessment compared to overall accuracy (Li & Chen, 2005). In the kappa coefficient, a value of 0 means no agreement exists while a value of 1 indicates a perfect agreement (Tang et al., 2015). In this study, the performance of models was assessed based on criteria proposed by Landis and Koch (1977). Specifically, the performance of models was divided into five categories: poor (kappa<0), slight (kappa: 0-0.2), fair (kappa: 0.21-0.40), moderate (kappa: 06.1-0.8), almost perfect (kappa: 0.81-1).

Both the overall accuracy and kappa coefficient of different classified rapeseed maps will be compared for the significant difference by pairwise z-statistics (Congalton, 1991). The result will be regarded as statistically significantly different when z value larger or equal to 1.96 (95% confidence level). Consider the pixel-based classification method used in this study, to make sure classified rapeseed maps in 2017 and

2019 are comparable, an additional McNemar's test was applied, the result will be regarded as statistically different when chi-square greater than 3.84 (95% confidence level, degree of freedom=1).

3. RESULTS

3.1. Temporal Behavior of Sentinel-1 Radar Signatures Over Rapeseed Fields

From Figure 11 to Figure 14 shows the box and whisker plot of Sigma VH, Sigma VV, VV-VH, and NDPI from October 7th of 2018 to June 4th of 2019, 21 images in total. For each step the observed 180 values of a related parameter included.

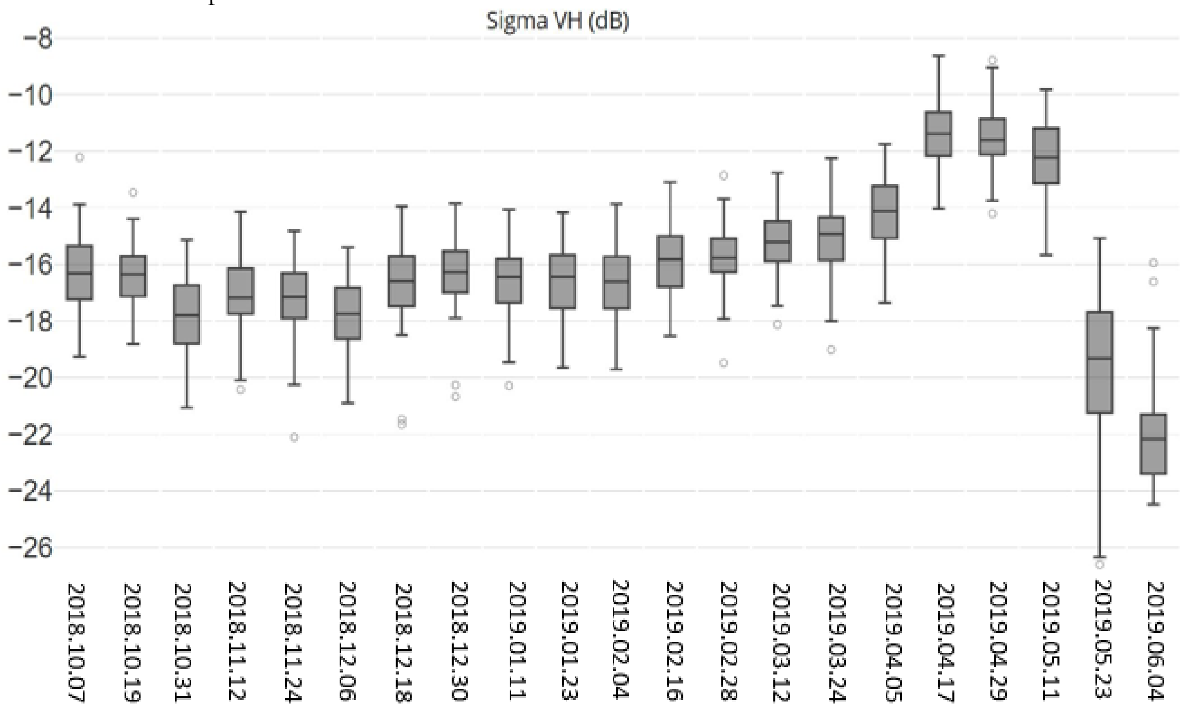

Figure 11 Box plot temporal profiles of Sigma VH

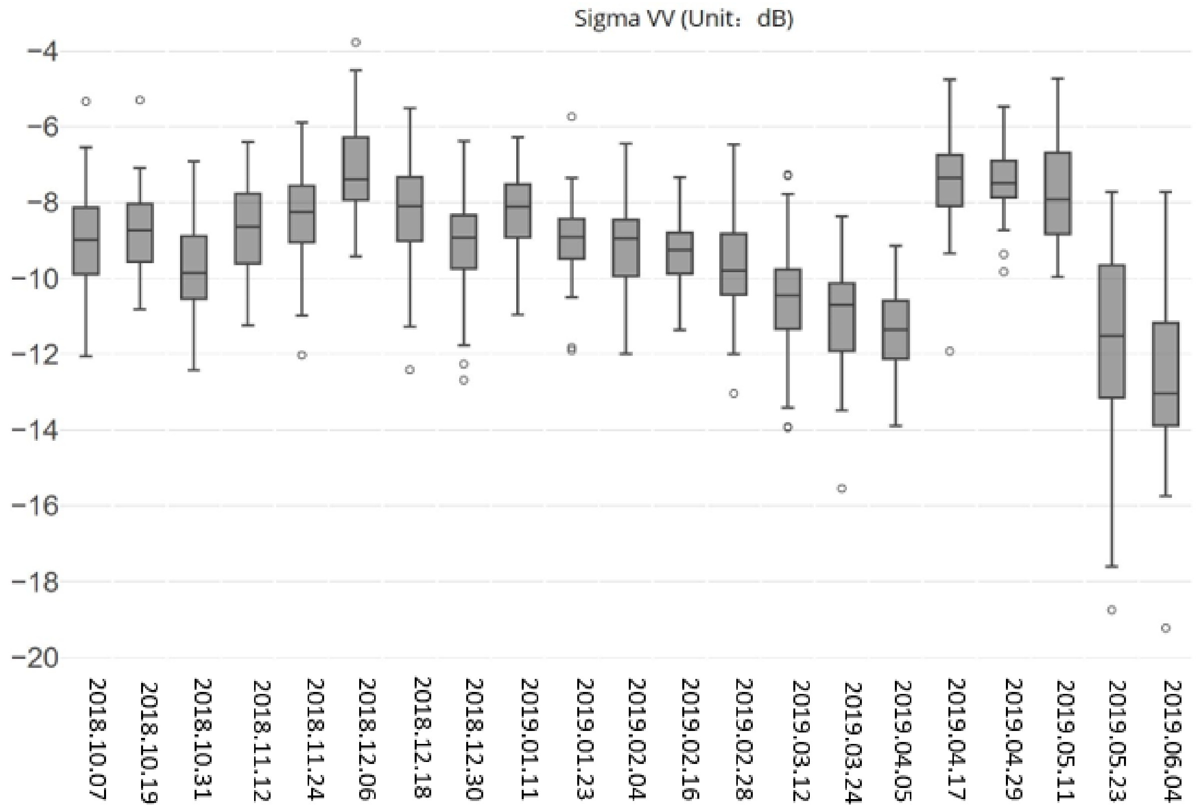

Figure 12 Box plot temporal profiles of Sigma VV

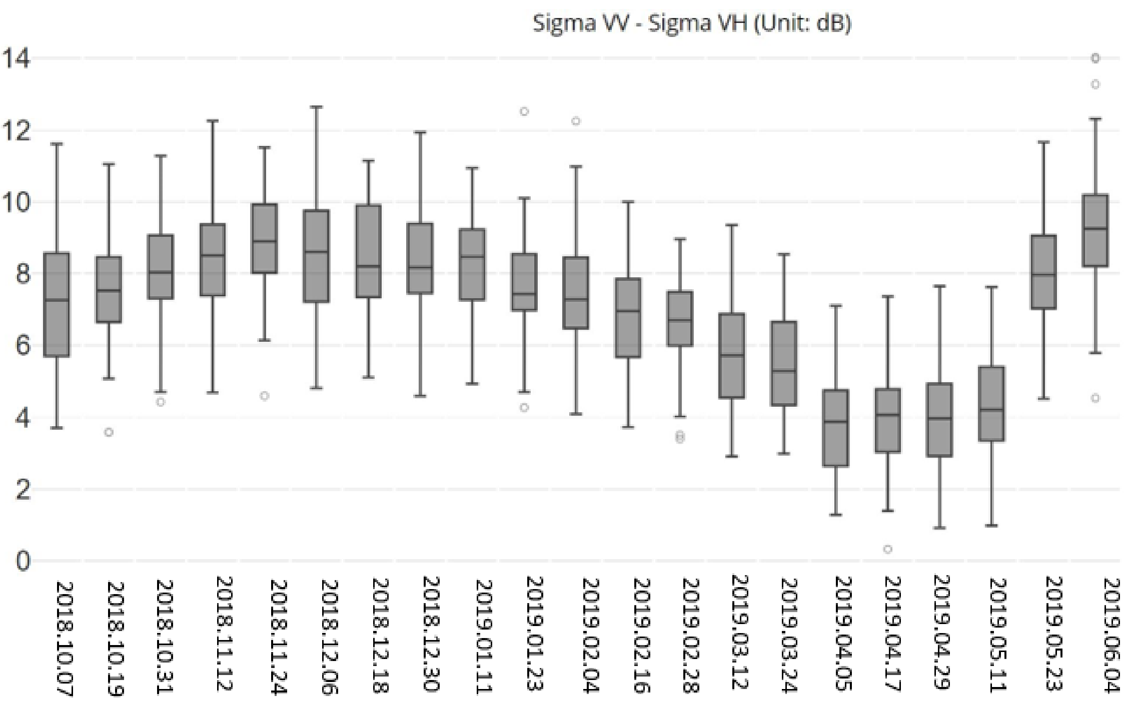

Figure 13 Box plot temporal profiles of Sigma VV – Sigma VH

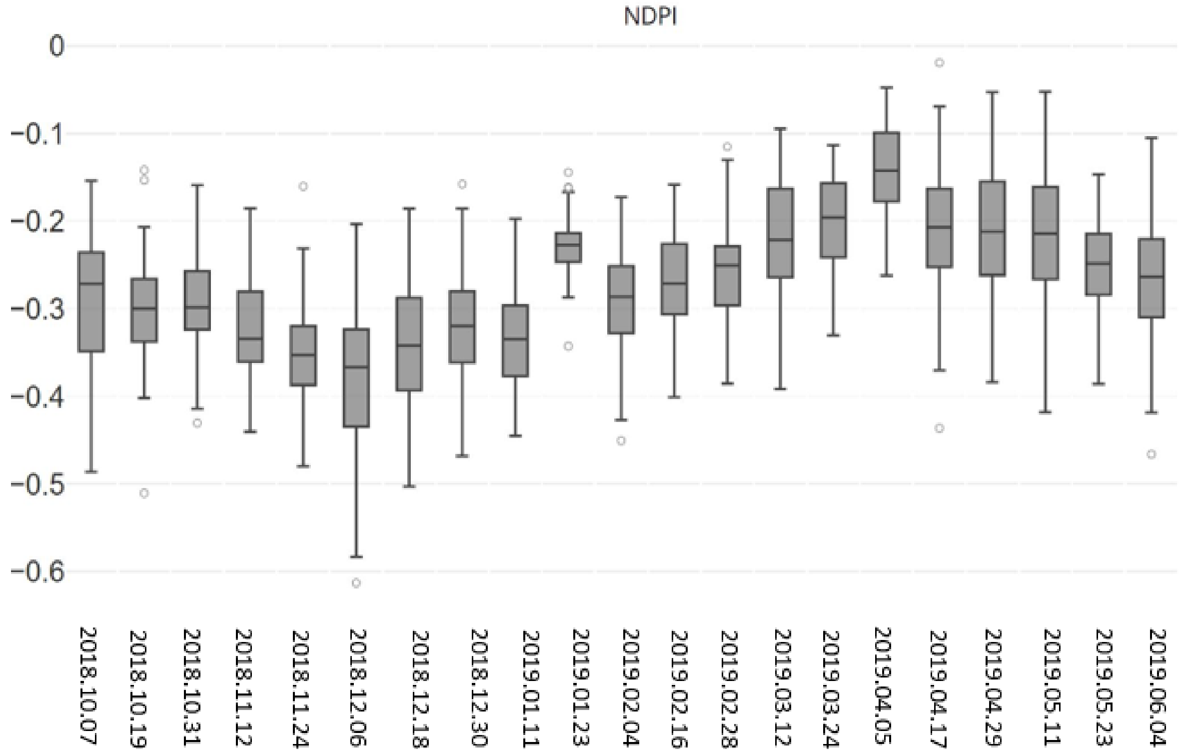

Figure 14 Box plot temporal profiles of NDPI

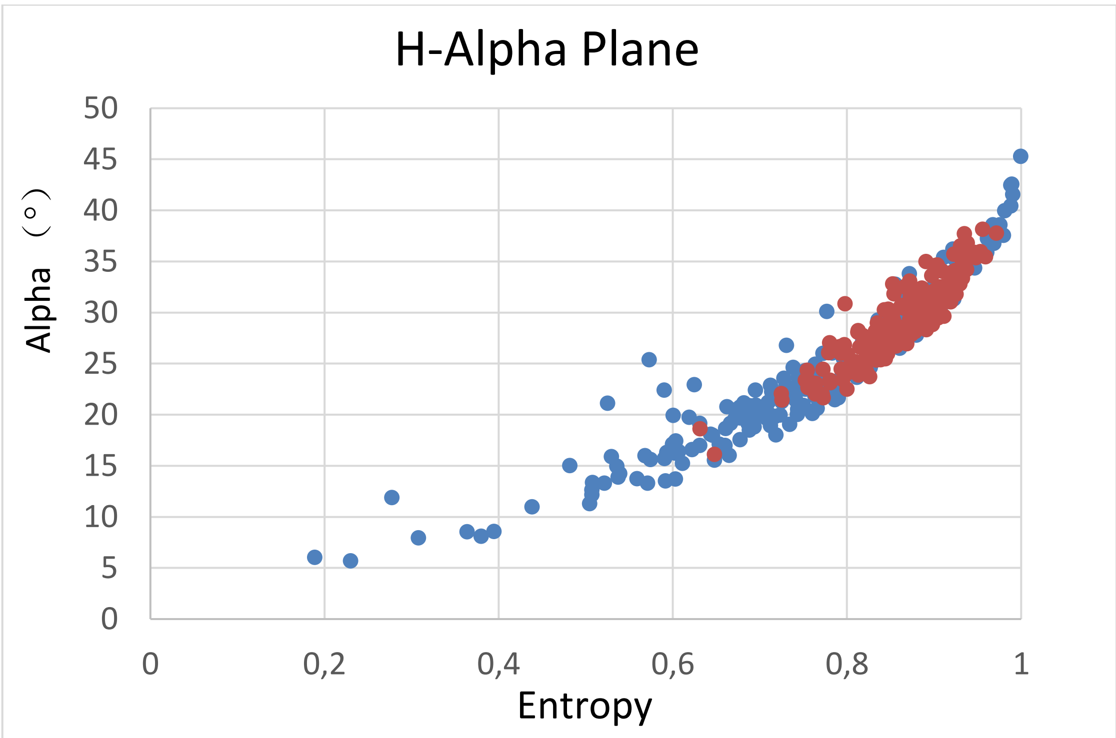

Figure 15 H-Alpha plane in 11th of May (figure illustrate rapeseed for the yellow color, non-rapeseed for blue color)

As shown in Figure 15, the entropy of rapeseed points mainly distributed in the range between 0.8-1 while the alpha mainly distributed in the range between 20-40, indicated that on the 11th of May in the Hanzhong basin, the dominant scattering mechanisms of rapeseed fields are medium-high entropy surface scattering (Table 2).

3.2. Classifier comparison for mapping rapeseed fields using Sentinel-1 time series

3.2.1. Random forest classification

According to the confusion matrix (Table 3), the overall accuracy was 99.1% and the kappa coefficient was 0.98, Indicated an almost perfect performance model performance proposed by Landis and Koch (1977).

Table 3 Confusion matrix of the classification result using Sentinel-1 time-series data through random forest classifier

Referenced data

Classifier data	Non-rapeseed	Rapeseed	Total	User accuracy
Non-rapeseed	54	1	55	98.18%
rapeseed	0	54	54	100%
Total	54	55	109	
Producer accuracy	100%	98.18%		

Overall accuracy = 99.1%

Kappa statistic = 0.98

3.2.2. Support vector machine classification

According to the confusion matrix (Table 4), the overall accuracy was 99.1% and the kappa coefficient was 0.98, Indicated an almost perfect performance model performance proposed by Landis and Koch (1977).

Table 4 Confusion matrix of the classification result using Sentinel-1 time-series data through support vector machine classifier

Referenced data

Classifier data	Non-rapeseed	Rapeseed	Total	User accuracy
Non-rapeseed	53	0	53	100%
rapeseed	1	55	56	98.21%
Total	54	55	109	
Producer accuracy	98.18%	100%		

Overall accuracy = 99.1%
Kappa statistic = 0.98

3.2.3. Accuracy comparison

Table 5 The Z-statistic comparison of random forest and support vector machine for rapeseed mapping in the Hanzhong basin

Classification method	Random forest	Support vector machine
Random forest	-	
Support vector machine	0	-

The result of Z-statistic is smaller than 1.96 (95% confidence level), indicates that there is no significant difference between classification accuracies of random forest and support vector classifier in rapeseed mapping using Sentinel-1 time-series data.

3.3. Variable importance

The Gini index displayed in Table 1 shows the variable importance of the Random Forest classifier when using the entire 21 images as input. According to Table 1, the Sigma VH value from April 17th of 2019 contributes the most to the classification, followed by anisotropy and entropy of the same day while the Aspect value on December 30th of 2019 contributes the least to the classification accuracy.

Table 6 Variable importance plot of classification result using time-series Sentinel-1 SAR data based on Gini index

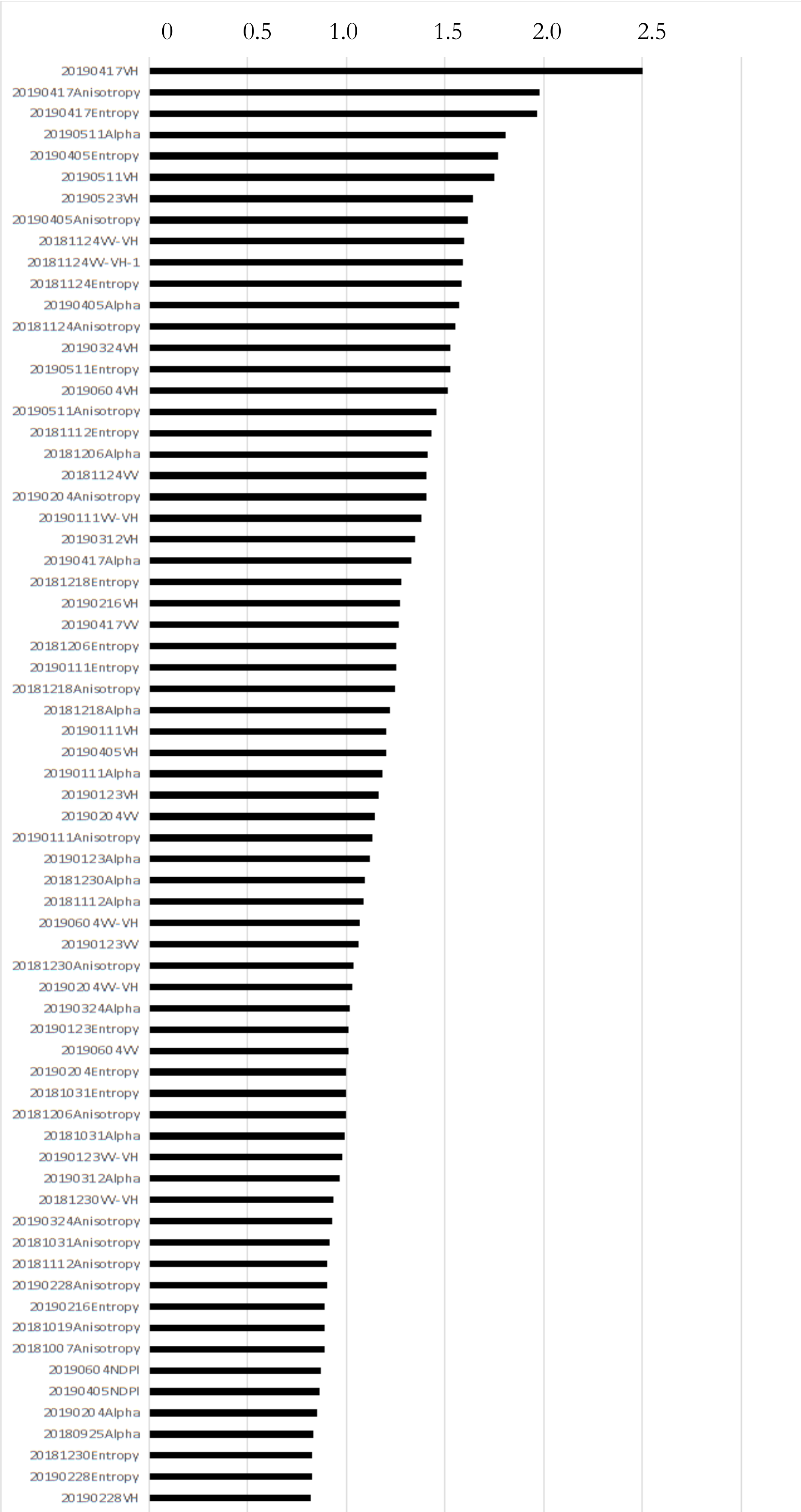

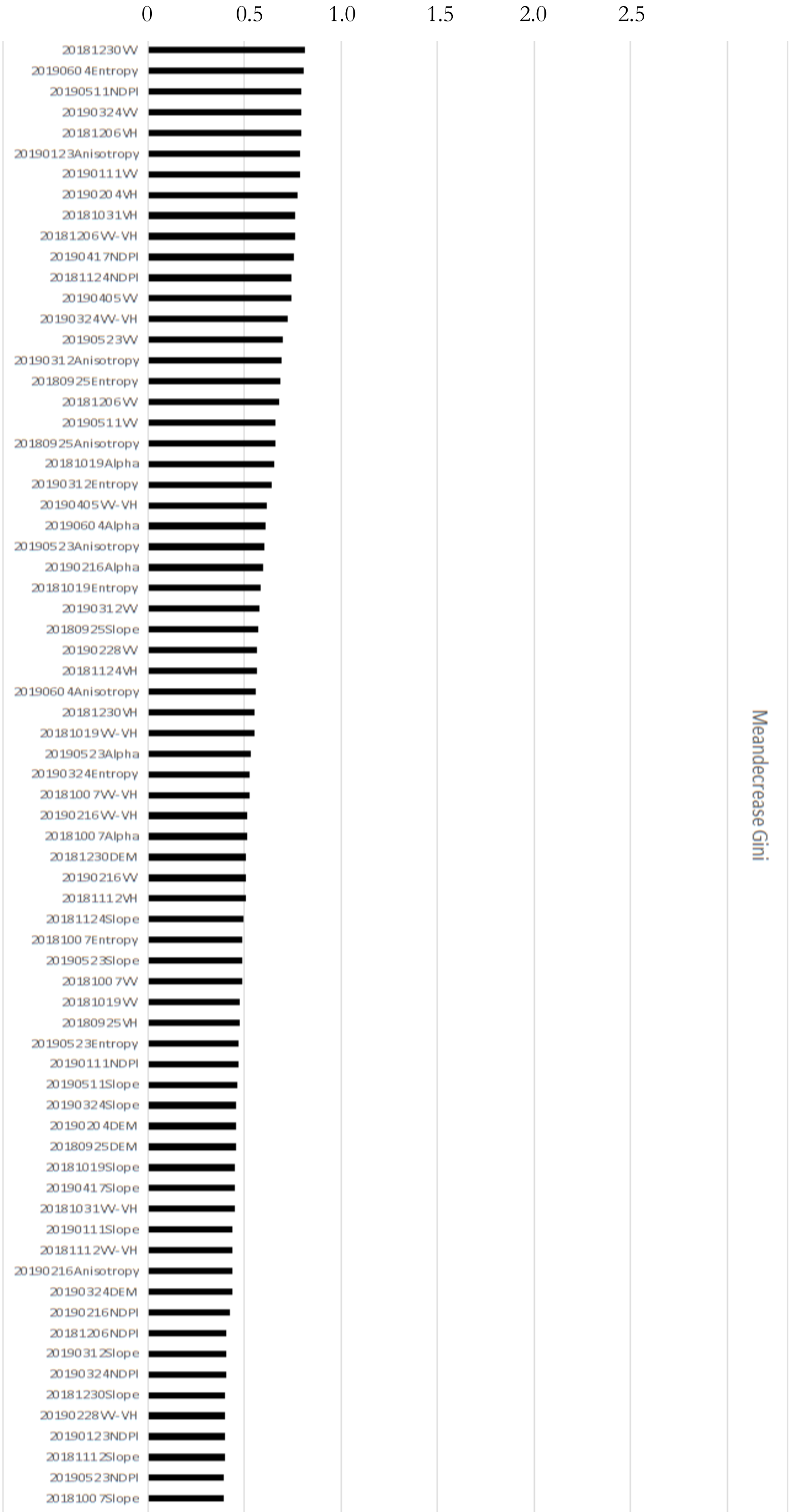
0
0.5
1.0
1.5
2.0
2.5
20181230VV
20190604Entropy
20190511NDPI
20190324VV
20181206VH
20190123Anisotropy
20190111VV
20190204VH
20181031VH
20181206VV-VH
20190417NDPI
20181124NDPI
20190405VV
20190324VV-VH
20190523VV
20190312Anisotropy
20180925Entropy
20181206VV
20190511VV
20180925Anisotropy
20181019Alpha
20190312Entropy
20190405VV-VH
20190604Alpha
20190523Anisotropy
20190216Alpha
20181019Entropy
20190312VV
20180925Slope
20190228VV
20181124VH
20190604Anisotropy
20181230VH
20181019VV-VH
20190523Alpha
20190324Entropy
20181007VV-VH
20190216VV-VH
20181007Alpha
20181230DEM
20190216VV
20181112VH
20181124Slope
20181007Entropy
20190523Slope
20181007VV
20181019VV
20180925VH
20190523Entropy
20190111NDPI
20190511Slope
20190324Slope
20190204DEM
20180925DEM
20181019Slope
20190417Slope
20181031VV-VH
20190111Slope
20181112VV-VH
20190216Anisotropy
20190324DEM
20190216NDPI
20181206NDPI
20190312Slope
20190324NDPI
20181230Slope
20190228VV-VH
20190123NDPI
20181112Slope
20190523NDPI
20181007Slope
Meandecrease Gini

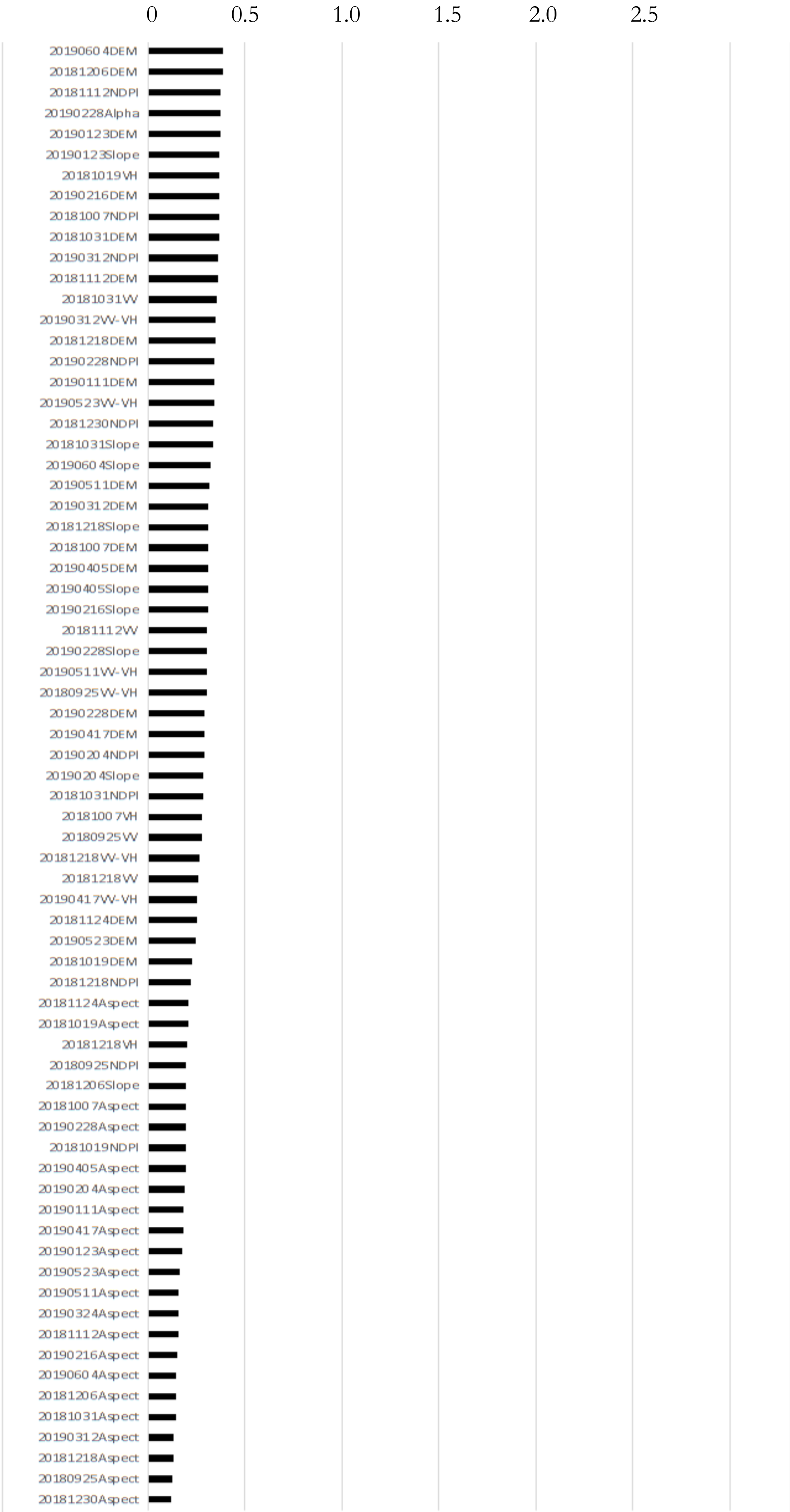
0
0.5
1.0
1.5
2.0
2.5
20190604DEM
20181206DEM
20181112NDPI
20190228Alpha
20190123DEM
20190123Slope
20181019VH
20190216DEM
20181007NDPI
20181031DEM
20190312NDPI
20181112DEM
20181031VV
20190312VV-VH
20181218DEM
20190228NDPI
20190111DEM
20190523VV-VH
20181230NDPI
20181031Slope
20190604Slope
20190511DEM
20190312DEM
20181218Slope
20181007DEM
20190405DEM
20190405Slope
20190216Slope
20181112VV
20190228Slope
20190511VV-VH
20180925VV-VH
20190228DEM
20190417DEM
20190204NDPI
20190204Slope
20181031NDPI
20181007VH
20180925VV
20181218VV-VH
20181218VV
20190417VV-VH
20181124DEM
20190523DEM
20181019DEM
20181218NDPI
20181124Aspect
20181019Aspect
20181218VH
20180925NDPI
20181206Slope
20181007Aspect
20190228Aspect
20181019NDPI
20190405Aspect
20190204Aspect
20190111Aspect
20190417Aspect
20190123Aspect
20190523Aspect
20190511Aspect
20190324Aspect
20181112Aspect
20190216Aspect
20190604Aspect
20181206Aspect
20181031Aspect
20190312Aspect
20181218Aspect
20180925Aspect
20181230Aspect

3.4. Rapeseed mapping accuracy based on mono-temporal Sentinel-1 data

Figure 16 shows the classification result of rapeseed or non-rapeseed uses the Sentinel-1 SAR image obtained from the 17th of April only. The classification map illustrates rapeseed for green color while non-rapeseed for yellow color. Through visual interpretation, the rapeseed covered almost half of the area, also many forests in the mountain region and city areas were misclassified to rapeseed fields. The map appears noisy and distribution patterns of rapeseed fields are hard to be distinguished.

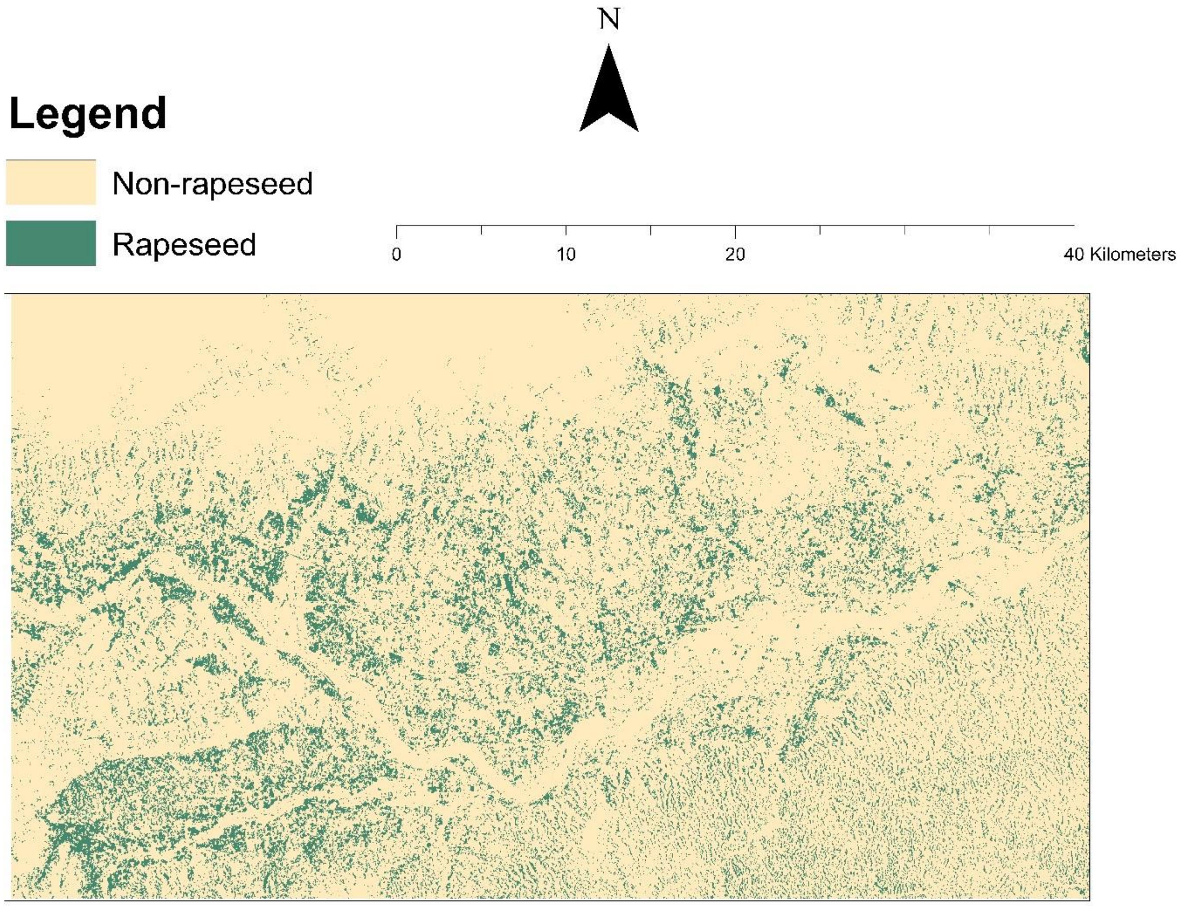

Figure 16 Classification result in the Hanzhong basin using mono-temporal Sentinel-1 image obtained on 17th of April, 2019 through random forest classifier

According to the confusion matrix (Table 7), the overall accuracy was 82.6% and the kappa coefficient was 0.65, Indicated a moderate performance model performance proposed by Landis and Koch (1977).

Table 7 Confusion matrix of the classification result using Sentinel-1 mono-temporal image obtained on April 17th, 2019 through random forest classifier

Referenced data				
Classifier data	Non-rapeseed	Rapeseed	Total	User accuracy
Non-rapeseed	41	6	47	87.23%
rapeseed	13	49	62	79.03%
Total	54	55	109	
Producer accuracy	75.93%	92.45%		

Overall accuracy = 82.57%
Kappa statistic = 0.65

Figure 17 shows the classification result of rapeseed or non-rapeseed use the Sentinel-1 SAR image obtained from the 11th of May only. Through visual interpretation, the map still appears noisy and distribution patterns of rapeseed fields are hard to be distinguished. Still, many forests in the mountain region and urban areas were misclassified into rapeseed fields.

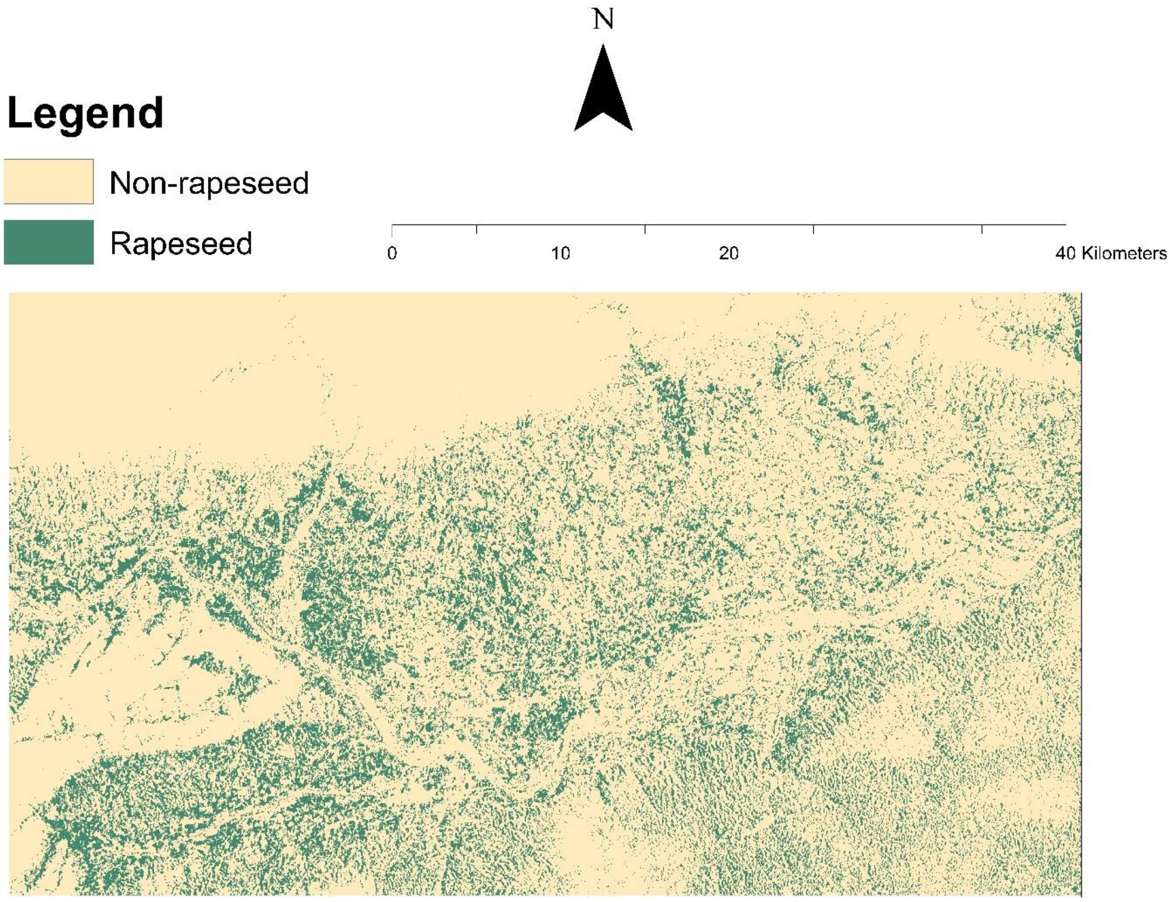

Figure 17 Classification result in the Hanzhong basin using mono-temporal Sentinel-1 image obtained on May 11th, 2019 through random forest classifier

According to the confusion matrix (Table 8), the overall accuracy was 99.1% and the kappa coefficient was 0.68, Indicated moderate performance model performance proposed by Landis and Koch (1977).

Table 8 Confusion matrix of the classification result using Sentinel-1 mono-temporal image obtained on 11th of May, 2019 through random forest classifier

Referenced data				
Classifier data	Non-rapeseed	Rapeseed	Total	User accuracy
Non-rapeseed	43	6	49	87.23%
rapeseed	11	49	60	79.03%
Total	54	55	109	
Producer accuracy	75.93%	92.45%		

Overall accuracy = 84.40%
Kappa statistic = 0.68

3.5. Rapeseed mapping accuracy based on multi-temporal Sentinel-1 data

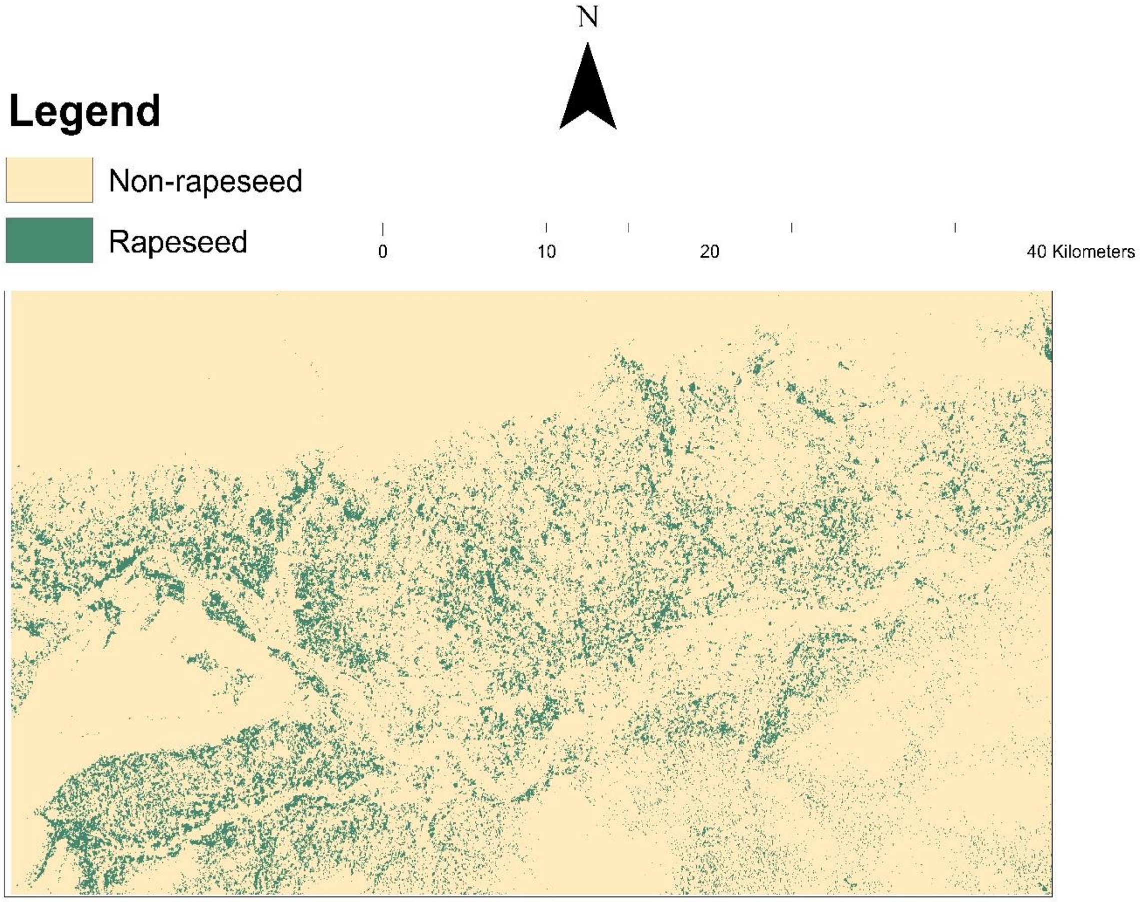

Figure 18 Classification result in the Hanzhong basin using multi-temporal Sentinel-1 images obtained on April 17th and May 11th of 2019 through random forest classifier

Figure 18 shows the classification result of rapeseed or non-rapeseed use multi-temporal Sentinel-1 SAR images obtained from April 17th and May 11th. Through visual interpretation, the misclassified in terms of forests and urban areas occurs less often compared to the results of using mono-temporal data. The distribution pattern of rapeseed can be distinguished preliminarily.

Table 9 Confusion matrix of the classification result using Sentinel-1 multi-temporal image obtained on April 17th and May 11th of 2019 through random forest classifier

Referenced data				
Classifier data	Non-rapeseed	Rapeseed	Total	User accuracy
Non-rapeseed	53	7	60	88.33%
rapeseed	1	48	49	97.96%
Total	54	55	109	
Producer accuracy	98.14%	87.27%		

Overall accuracy = 92.66%
Kappa statistic = 0.85

According to the confusion matrix (Table 9), the overall accuracy was 92.66% and the kappa coefficient was 0.85, Indicated an almost perfect performance model performance proposed by Landis and Koch (1977).

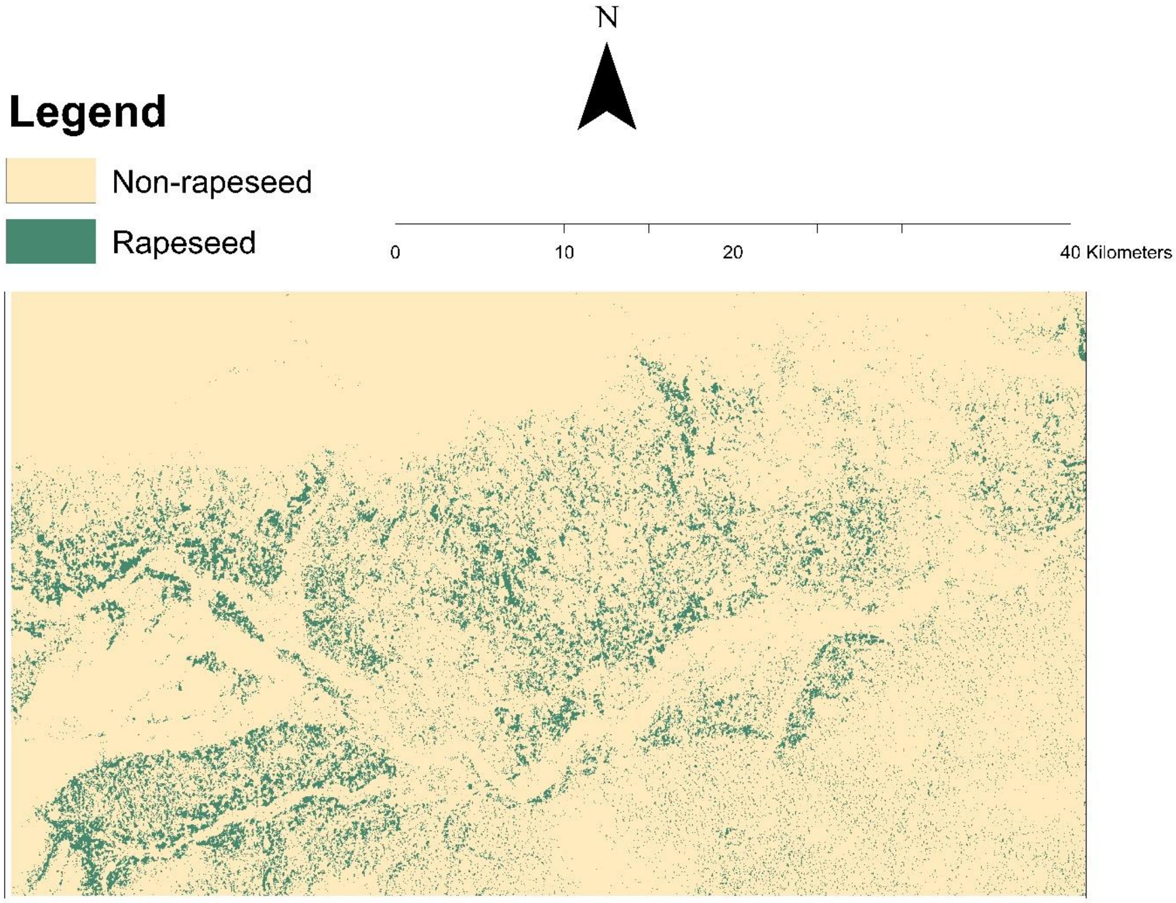

Figure 19 Classification result in the Hanzhong basin using multi-temporal Sentinel-1 images obtained on April 17th, May 11th, and Map 23rd of 2019 through random forest classifier

Figure 19 shows the classification result of rapeseed or non-rapeseed use multi-temporal Sentinel-1 SAR images obtained from April 17th, May 11th, and Map 23rd of 2019. This classification map has a better performance compared to classifier maps shown before, only a few urban areas were misclassified as rapeseed fields.

Table 10 Confusion matrix of the classification result using Sentinel-1 multi-temporal image obtained on April 17th, May 11th, and May 23rd of 2019 through random forest classifier

Referenced data				
Classifier data	Non-rapeseed	Rapeseed	Total	User accuracy
Non-rapeseed	51	2	53	96.23%
rapeseed	3	53	56	94.64%
Total	54	55	109	
Producer accuracy	94.44%	96.36%		

Overall accuracy = 95.41%
Kappa statistic = 0.91

According to the confusion matrix (Table 10), the overall accuracy was 95.41% and the kappa coefficient was 0.91, Indicated an almost perfect performance model performance proposed by Landis and Koch (1977).

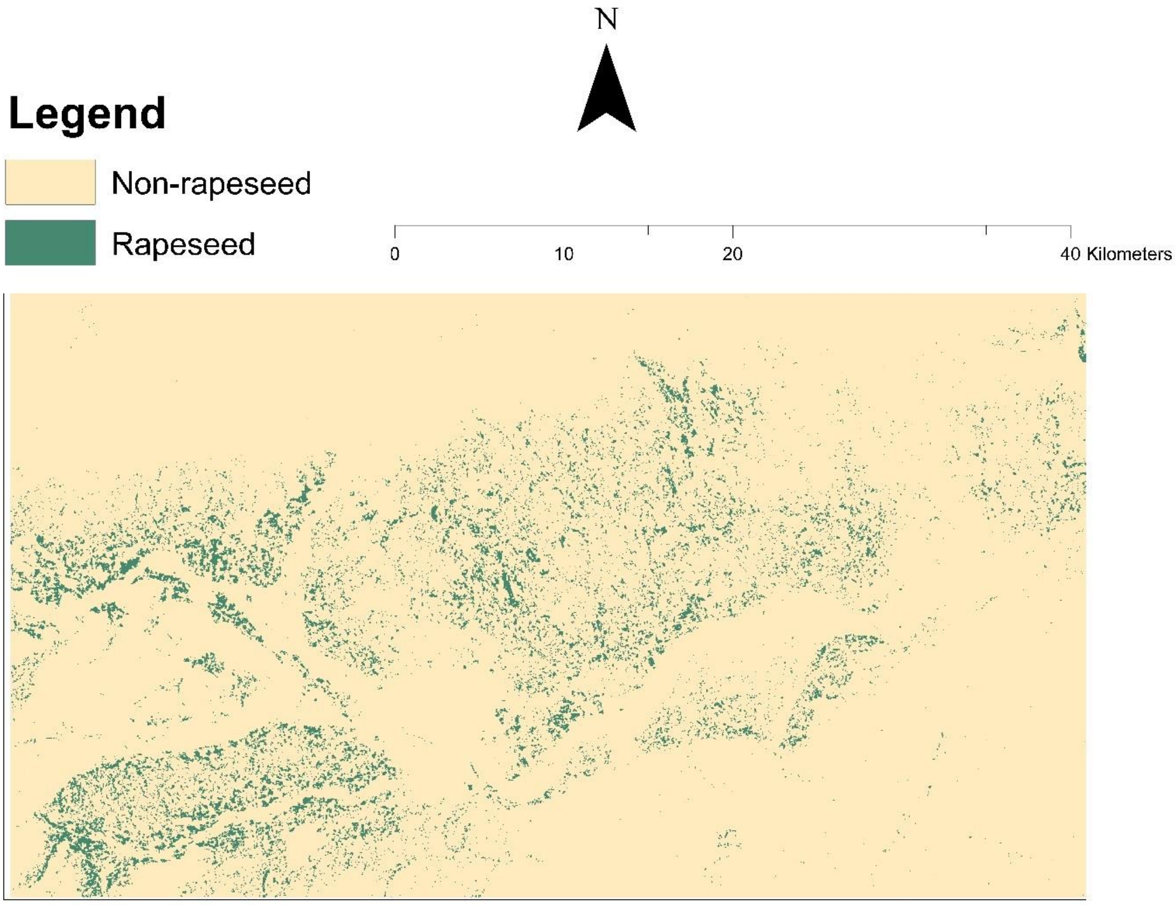

Figure 20 Classification result in the Hanzhong basin using multi-temporal Sentinel-1 images obtained on April 5th, April 17th, April 29th, May 11th, and Map 23rd of 2019 through random forest classifier

Figure 20 shows the classification result of rapeseed or non-rapeseed use multi-temporal Sentinel-1 SAR obtained on April 5th, April 17th, April 29th, May 11th, and Map 23rd of 2019. Obviously, this map performance better than mono-temporal images or other multi-temporal images. The boundary of urban areas can be easily distinguished which means the misclassified problem related to urban areas was solved. Also, only a few rapeseed fields occurred in the mountain region which conforms to the facts that rapeseed also planted in the relatively flat area inside the mountain region.

Table 11 Confusion matrix of the classification result using Sentinel-1 multi-temporal image obtained on April 17th, May 11th, and May 23rd of 2019 through random forest classifier

Referenced data

Classifier data	Non-rapeseed	Rapeseed	Total	User accuracy
Non-rapeseed	52	1	53	96.23%
rapeseed	2	54	56	94.64%
Total	54	55	109	
Producer accuracy	94.44%	96.36%		

Overall accuracy = 97.24%
Kappa statistic = 0.94

According to the confusion matrix (Table 11), the overall accuracy was 97.24% and the kappa coefficient was 0.94, Indicated an almost perfect performance model performance proposed by Landis and Koch (1977).

Table 12 The z-statistic comparison of selected temporal combinations for rapeseed mapping in the Hanzhong basin. Significantly different accuracies with 95% confidence interval are indicated by *

Temporal dimensions	Mono-temporal April 17	Mono-temporal May 11	Multi-temporal (2 images)	Multi-temporal (3 images)	Multi-temporal (5 images)	Time-series
Mono-temporal April 17						
Mono-temporal May 11	0.36					
Multi-temporal (2 images)	2.26*	1.91				
Multi-temporal (3 images)	3.02*	2.70*	0.86			
Multi-temporal (5 images)	3.59*	3.28*	1.54	0.72		
Time-seris	4.22*	3.93*	2.38*	1.66	1.00	

3.6. Change Detection of Rapeseed Field Between 2017 and 2019

3.6.1. Classification of rapeseed fields in 2017

Figure 21 shows the classification result of rapeseed or non-rapeseed use multi-temporal Sentinel-1 SAR images obtained on April 3, April 15, April 27, May 9, and May 21 of 2017. Similar to Figure 20, the distribution pattern of rapeseed fields can be distinguished.

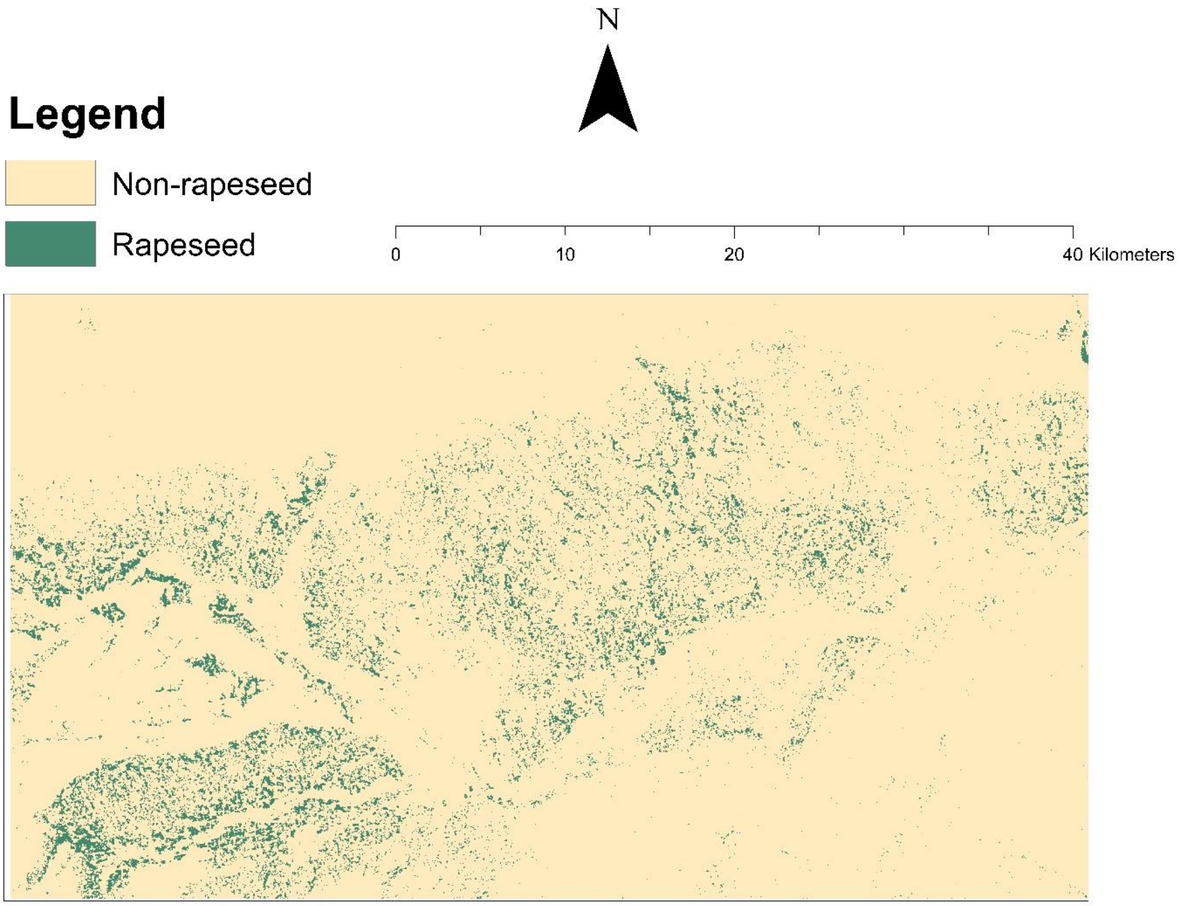

Figure 21 Classification result in the Hanzhong basin using multi-temporal Sentinel-1 images obtained on April 3, April 15, April 27, May 9, and May 21 of 2017 through random forest classifier

Table 13 Confusion matrix of the classification result using Sentinel-1 multi-temporal image obtained on April 3, April 15, April 27, May 9, and May 21 of 2017 through random forest classifier

Referenced data				
Classifier data	Non-rapeseed	Rapeseed	Total	User accuracy
Non-rapeseed	53	2	55	96.36%
rapeseed	1	53	54	98.14%
Total	54	57	109	
Producer accuracy	98.14%	92.98%		

Overall accuracy = 97.24%
Kappa statistic = 0.94

According to the confusion matrix (Table 13), the overall accuracy was 97.24% and the kappa coefficient was 0.94, Indicated an almost perfect performance model performance proposed by Landis and Koch (1977).

Table 14 and 15 shows the classification accuracy of rapeseed fields in the Hanzhong basin in 2017 and 2019 using additional 120 validation points respectively. Both of these two results indicated as almost perfect model performance.

Table 14 Confusion matrix of classification using addition 120 validation points of 2017

Classifier data	Non-rapeseed	Rapeseed	Total	User accuracy
Non-rapeseed	58	0	58	100%
rapeseed	2	60	62	96.78%
Total	60	60	120	
Producer accuracy	96.67%	100%		

Overall accuracy = 98.33%
Kappa statistic = 0.96

Table 15 Confusion matrix of classification using addition 120 validation points of 2019

Classifier data	Non-rapeseed	Rapeseed	Total	User accuracy
Non-rapeseed	58	1	59	98.30%
rapeseed	2	59	61	96.72%
Total	60	60	120	
Producer accuracy	96.67%	98.33%		

Overall accuracy = 97.50%
Kappa statistic = 0.95

Table 16 z-statistic and Chi-square of McNemar's test

Chi-square	0.33
Z-statistic	0.14

As shown in Table 16, the z-statistic between classification result between 2017 and 2019 is 0.14 (<1.96, 95% confidence level) while Chi-square is 0.33 (<3.84, 95% confidence level, df= 1), indicated that there is no test of significant differences of classification accuracy between rapeseed distribution maps in 2017 and 2019.

3.6.2. Change detection

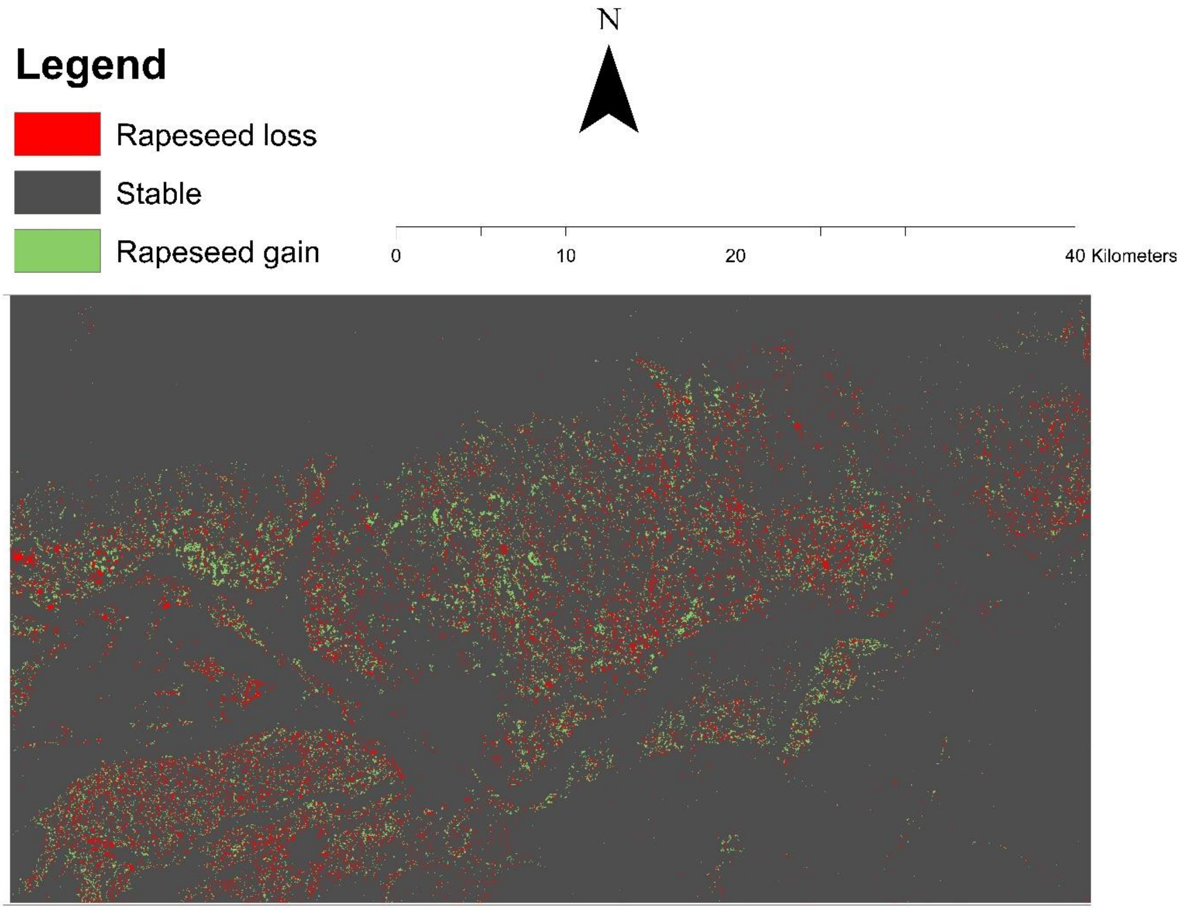

Figure 22 Change detection map of rapeseed fields in the Hanzhong basin between 2017 and 2019

Figure 22 shows the change of rapeseed fields in the Hanzhong basin between 2017 and 2019. The change detection map illustrated rapeseed fields loss for red, stable areas for grey, and rapeseed gain for green. Through visual interpretation, a rapid change of rapeseed fields can be found. Moreover, a huge increase in rapeseed fields can be found in the middle and middle west part of the Hanzhong basin. According to the pixel-based statistic, the total area of rapeseed fields in the Hanzhong basin was 134.39km^2 in 2017, and 128.39 km^2 in 2019 which means the area of rapeseed fields in the Hanzhong basin decreased 6km^2.

4. DISCUSSION

4.1. Accuracy and feasibility of Sentinel-1 SAR data for mapping rapeseed fields

This study accesses the capacity for Sentinel-1 dual-polarization SAR data for rapeseed mapping and monitoring. Twenty-one Sentinel-1 images in 2019 were acquired, and both pixel-based random forest and support vector machine classifiers were performed on these data. The classification results led to an overall accuracy of 99.1%, and a kappa coefficient of 0.98 in both the random forest model and support vector machine model. Compared to the result of Vaudour et al. (2015) (87% Overall accuracy) and Wang et al. (2018) (85% overall accuracy) and many other studies that only used optical imagery in rapeseed mapping, this study achieved higher classification accuracy (Waldhoff et al., 2017; Esch et al., 2014). Furthermore, the rainy (cloudy) weather condition, which frequently occurs at growth stages of rapeseed encourages the use of Sentinel-1 data in rapeseed mapping. Also, compared to many other studies that used combinations of Sentinel-1 and optical images in monitoring rapeseed, this study gets a similar classification accuracy without adding additional optical imagery (Mercier et al., 2020; Lussem et al., 2016). The reason may be as follows: only the central points of rapeseed fields that reached 50m x 50m size were selected and thanks to homogeneous rapeseed fields, rich backscatter information was provided. At the same time, it was easier to distinguish rapeseed fields. The regular and distinct land rotations of rapeseed in the Hanzhong basin make the backscatter signal observable, thus contributing to the classification. The results of this study proved the potential of Sentinel-1 data for rapeseed mapping.

From the result kappa z-test, it can be found that there is no significant difference among the classification resulted from either the use of random forest classifier or the use of support vector machine classifier. In studies that used Sentinel-1 data in land cover classification (Jamali, 2020), urban area extraction (Jamali and Rahman, 2019) through random forest and support vector machine classifiers also showed similar results. This Proves that the Sentinel-1 data is not sensitive to these two classifiers.

Thanks to the significant correction between SAR backscatter coefficients with rapeseed growth stages (Zhang et al., 2018), this study achieved a high classification accuracy. VH, VV remain stable before rosette. During the rosette and bud stage, the value of VH and VV slightly increases with the rapeseed growth as well as the increase in biomass. During flowering (start of March-start of April), VH keeps increasing while VV starts decreasing gradually. The trend of decreasing in VV can be explained by the decrease of vertical transformation from dense rosette to a thin flowering stalk. Both VV and VH showed a dramatic increase at the start of ripening (start of April-mid of May), which was also observed in many other studies (Wiseman et al., 2014; Fieuzal et al ., 2013). The increase was caused by the huge development of rapeseed structure while stems have no preferred orientations during this period. This leads to more complex geometry and results in a strong volume-scattering (Betbeder et al., 2016). During ripening (mid of April-start of May), both VV and VH showed a slight decrease attributable to the reduction of water content in both the soil and the top layer of rapeseed. Similar results were also found in many other studies (Mercier et al., 2020; Veloso et al., 2017). After harvesting (mid of May-start of June), both VV and VH decreased dramatically. The selected backscatter indices VV-VH showed an opposite trend compared to VV and VH, while the NDPI changed rapidly through growth stages. Therefore, it is hard to explain the correction between VV-VH and NDPI with rapeseed growth stages.

As shown in Figure 15, the Entropy-Alpha plane indicated that on the 11th of May in the Hanzhong basin, the dominant scattering mechanisms of rapeseed fields are medium-high entropy surface scattering. However, according to the local crop calendar (Figure 8), the rapeseed is in the ripening stage during this period which means the vegetation volume scattering should be the dominant scattering mechanism. This may be caused by less information related to scattering objects that can be provided by dual-polarization compared to full-polarimetric data (Sugimoto et al., 2013). Similiar, Li and Bijker (2019) summarized that, in Sentinel-1 imagery, Sigma VV and Sigma VH are robust in vegetable classification while features acquired through decomposition did not add additional value to the classification result.

4.2. Optimal timing for mapping rapeseed fields using Sentinel-1 SAR data

Despite the high classification accuracy provided by the use of Sentinel-1 time-series images in the rapeseed classification, the huge size of the entire dataset (21 images, containing 210 bands in total) limited the implementation of the classification. To reduce the input data size, the performance of using mono-temporal and multi-temporal Sentinel-1 images in rapeseed classification has been explored and compared.

The variable importance, an essential concept in machine learning classification models, provides a scientific way in both understanding and explaining models. In this study, all variables were retrieved from Sentinel-1 data and DEM data, indicated the biomass production, vegetation structure, moisture content, and topographic information of rapeseed fields. According to the variable importance table, DEM, slope, and aspect generated from DEM data contribute the least to the classification, which is understandable because DEM data is regarded as supportive data assumed no change in 2019. Within each day, Sigma VH and SigmaVV more likely to get the highest Gini value to conform with the previous conclusion that Sigma VH and Sigma VV closely related to the growth of rapeseed.

According to the variable importance table, the importance of variables provided by April and May 2019 contributes most to RF classification. Among them, the variables retrieved from April 17 of 2019, and May 11 of 2019 contribute the most to the classification result. Hence, to reduce the input data size, the classification performance of mono-temporal (17th of April, 11th of May) and multi-temporal were displayed and compared. The result showed classification accuracies of using two mono-temporal images are significantly lower than that using time-series images. This was caused by less information on growth stages that can be provided by mono-temporal images compared to time-series images. The classification accuracies of multi-temporal using two or three images are higher than that using mono-temporal images. Especially when the image obtained on the 23rd of May added because the sharp change of rapeseed fields between before and after harvesting was captured. The classification accuracy (overall accuracy= 95.41, kappa statistic= 0.91) of using multi-temporal that contains three images (17th of April, 11th of May, 23rd of May) has no significant differences compared to that using time-series images. However, the classified rapeseed distribution did not match the high-resolution optical images perfectly. This circumstance may be caused by the selection of sample points. In the sample points selection, only the central pixels of the rapeseed fields reaching 50mx50m size were selected. Thus, the classification accuracy only showed whether the central pixels of the rapeseed fields were correctly classified rather than whether entire rapeseed fields were correctly classified. The lack of image segmentation and the inability to generate homogenous image objects' is the main disadvantage of pixel-based classification over object-based classification (Liu, et al. 2010). By contrast, rapeseed fields extraction using all 5 images obtained in April and May of 2019, achieved the highest classification accuracy among the use of multi-temporal images, and the classified results matched the rapeseed fields in the high-resolution optical image almost perfectly. In Sentinel-1 data obtained from April and May, backscatter information related to the end of the flowering stage, the ripening stage, and the harvesting stage can be provided. Unique structural changes of rapeseed in these stages were captured, therefore achieved a high classification accuracy.

It is also worth mentioning that despite features acquired from the 17th of April contribute the most to the classification result. The classification accuracy (overall accuracy = 82.57%, kappa statistic = 0.65) of using the image obtained on the 17th of April is lower than that use the image obtained on the 11th of May (overall accuracy = 84.40%, kappa statistic = 0.68). The dramatic change in both Sigma VV and Sigma VH between the 5th of April and 17th of April was captured by the classifier, therefore get high rank in mean decrease Gini.

4.3. Spatial and temporal changes of rapeseed fields in the Hanzhong Basin

Indicated by the change map of rapeseed between 2017 and 2019, the total size of the rapeseed field in 2019 is 6 km^2 less than that in 2017, which means the rapeseed fields in the Hanzhong basin remains stable between 2017 and 2019.

The change detection map shows a high frequency of land rotation. The land rotation can be regarded as an effective way of both controlling the pest problems as well as a remedy for soil productivity (Spencer, et al.2008). In the Hanzhong basin, the rapeseed field is mainly rotated with the wheat field, which proved a mature way of land management in the Hanzhong basin, it maximizes the productivity of the field and reduces the impact of pests while meeting the primary yield supply of both wheat and rapeseed.

The Hanzhong basin transformed into a vast sea of rape flowers from mid-March to mid-April, known as the most beautiful rape flower sea in China. The extraordinary scenery of the broad area of rape flowers attracts thousands of tourists and becomes the most essential part of the local tourism industry. Thus, the "rape flower festival", dominated by the Hanzhong municipal government, aimed at through the medium of rape flowers and promote the development of local tourism emerged. "The main venue" was set up to highlight the theme "rape flower sea" of the festival and changed among counties annually. Rapeseed fields in a county tend to be more aggregated when hosting the main venue. Also, the size of the rapeseed fields where the main venue was located will increase. In 2017 the main venue was set in Mian county while in 2019 the Hantai district was hosting the festival. The change of the main venue explained the change of aggregated fields of rapeseed. In 2017 when the main venue set in the Mian county, the aggregated dense rapeseed fields occur in the north-west corner of the study area, while in 2019 the aggregated dense rapeseed fields occur in the central part of the study area. In consequence, the north-west corner of the change map shows a massive decline in aggregated rapeseed fields while in the central part, there is a considerable increase. Fitness between the rapeseed fields changed the map, and the actual situation also proved the accuracy of classification.

5. CONCLUSION AND RECOMMENDATIONS

5.1. Conclusion

In this study, rapeseed fields were mapping over Hanzhong Basin in Shaanxi Province, China using the Sentinel-1 SAR time series and digital terrain data by applying two classification algorithms: Random Forests and Support Vector Machine. The optimal timing for mapping rapeseed fields was investigated, and the changes of rapeseed fields in the study area between 2017 and 2019 were also quantified. The study showed that the Sentinel-1 SAR data can successfully be used to map rapeseed fields with a very high classification accuracy, no matter which classification algorithm was applied. The optimal timing for mapping rapeseed fields in Hanzhong Basin is in April and May. The rapeseed fields change hot spot was found to be consistent with the host place of the Rapeseed Flowers Festival in the study area, although a slight decline of the rapeseed fields, as well as a high frequency of crop rotation with other crops (i.e., winter wheat), has been observed between 2017 and 2019. Given the very good accuracy obtained and the fact that Sentinel-1 SAR data is free and open access, it is believed that the Sentinel-1 SAR time series may be used for mapping and monitoring of rapeseed fields over large areas such as national and continental levels.

5.2. Recommendation

Rapeseed plays an essential role in securing edible oil worldwide. Rapeseed fields in the Hanzhong basin were statistically analyzed with pixel-based random forest classifier. The results show a high classification accuracy. However, the marginal area of rapeseed fields did not be correctly classified occasionally. For further research, the object-based classification is suggested.

The capacity of Sentinel-1 backscatter coefficients was proved by this study, while features acquired from SAR decomposition contribute less to the classification. For further research, the use of backscatter coefficients is suggested, and, the use of Full-polarimetric data is suggested if decomposed features are needed.

LIST OF REFERENCES

Aschbacher, J., Pongsrihadulchai, A., Karnchanasutham, S., Rodprom, C., Paudya, D. R., & Toan, T. Le. (1995). Assessment of ERS-1 SAR data for rice crop mapping and monitoring, 83–85.

Atzberger, C. (2013). Advances in remote sensing of agriculture: Context description, existing operational monitoring systems and major information needs. *Remote Sensing*, *5*(2), 949–981. https://doi.org/10.3390/rs5020949

Belgiu, M., & Drăguţ, L. (2016). Random forest in remote sensing: A review of applications and future directions. ISPRS Journal of Photogrammetry and Remote Sensing, 114, 24–31. https://doi.org/10.1016/j.isprsjprs.2016.01.011

Bruzzone, L., Marconcini, M., Wegmüller, U., & Wiesmann, A. (2004). An advanced system for the automatic classification of multitemporal SAR images. IEEE Transactions on Geoscience and Remote Sensing, 42(6), 1321–1334. http://doi.org/10.1109/TGRS.2004.826821

Cao, Y.G., Yan, L.J., Zheng, Z.Z., 2008. Extraction of information on geology hazard from multi-polarization SAR images. The International Achieves of the Photogrammetry, Remote Sensing and Spatial Information Science 37, 1529–1532.

Chan, J. C.-W., Beckers, P., Spanhove, T., & Borre, J. Vanden. (2012). An evaluation of ensemble classifiers for mapping Natura 2000 heathland in Belgium using spaceborne angular hyperspectral (CHRIS/Proba) imagery. International Journal of Applied Earth Observation and Geoinformation, 18, 13–22.https://doi.org/10.1016/j.jag.2012.01.002

Chan, J. C.-W., & Paelinckx, D. (2008a). Evaluation of Random Forest and Adaboost tree-based ensemble classification and spectral band selection for ecotope mapping using airborne hyperspectral imagery. Remote Sensing of Environment, 112(6), 2999–3011. https://doi.org/10.1016/j.rse.2008.02.011

Chan, J. C.-W., & Paelinckx, D. (2008b). Evaluation of Random Forest and Adaboost tree-based ensemble classification and spectral band selection for ecotope mapping using airborne hyperspectral imagery. Remote Sensing of Environment, 112(6), 2999–3011. https://doi.org/10.1016/J.RSE.2008.02.011

Cai, Y., Lin, H., & Zhang, M. (2019). ScienceDirect Mapping paddy rice by the object-based random forest method using time series Sentinel-1 / Sentinel-2 data. *Advances in Space Research*. https://doi.org/10.1016/j.asr.2019.08.042

Choudhury, I., & CHAKRABORTY, M. (2006). SAR signature investigation of rice crop using RADARSAT data, (February 2006). https://doi.org/10.1080/01431160500239172

Cloude, S R, Goodenough, D. G., & Chen, H. (2012). Compact Decomposition Theory. *IEEE Geoscience and Remote Sensing Letters*, *9*(1), 28–32. https://doi.org/10.1109/LGRS.2011.2158983

Cloude, Shane Robert, & Pettier, E. (1996). A review of target decomposition theorems in radar polarimetry. *IEEE Transactions on Geoscience and Remote Sensing*, *34*(2), 498–518. https://doi.org/10.1109/36.485127

Cloutis, E. A. (1999). Agricultural crop monitoring using airborne multispectral imagery and C-band synthetic aperture radar, *1161*. https://doi.org/10.1080/014311699213181

Colditz, R. R. (2015). An evaluation of different training sample allocation schemes for discrete and continuous land cover classification using decision tree-based algorithms. *Remote Sensing*, *7*(8), 9655–9681. https://doi.org/10.3390/rs70809655

Congalton, R. G. (1991). A review of assessing the accuracy of classifications of remotely sensed data. Remote Sensing of Environment, 37(1), 35–46. https://doi.org/10.1016/0034-4257(91)90048-B

Cohen, J. (1960). A Coefficient of Agreement for Nominal Scales. Educational and Psychological Measurement, 20(1), 37–46. https://doi.org/10.1177/001316446002000104

Cookmartin, G., Saich, P., Quegan, S., Cordey, R., Burgess-Alien, P., & Sowter, A. (2000). Modeling microwave interactions with crops and comparison with ERS2 SAR observations. IEEE Transactions on Geoscience and Remote Sensing, 38(2 I), 658–670. https://doi.org/10.1109/36.841996

d'Andrimont, R., Taymans, M., Lemoine, G., Ceglar, A., Yordanov, M., & van der Velde, M. (2020). Detecting flowering phenology in oilseed rape parcels with Sentinel-1 and -2 time series. *Remote Sensing of Environment*, *239*(September 2019), 111660. https://doi.org/10.1016/j.rse.2020.111660

Denize, J., Hubert-Moy, L., Betbeder, J., Corgne, S., Baudry, J., & Pottier, E. (2019). Evaluation of using sentinel-1 and -2 time-series to identify winter land use in agricultural landscapes. *Remote Sensing*, *11*(1). https://doi.org/10.3390/rs11010037

Dong, J., & Xiao, X. (2016). Evolution of regional to global paddy rice mapping methods: A review. *ISPRS Journal of Photogrammetry and Remote Sensing*, *119*, 214–227. https://doi.org/10.1016/j.isprsjprs.2016.05.010

Esch, T., Metz, A., Marconcini, M., & Keil, M. (2014). The combined use of multi-seasonal high and medium resolution satellite imagery for parcel-related mapping of cropland and grassland. *International Journal of Applied Earth Observation and Geoinformation*, *28*(1), 230–237. https://doi.org/10.1016/j.jag.2013.12.007

European Space Agency (ESA), 2013. ESA Sentinel 1 handbook, European Space Agency technical note. doi:10.1017/CBO9781107415324.004

Evgeniou, T., & Pontil, M. (2014). Workshop on Support Vector Machines : Theory and Applications. *Machine Learning and Its Applications: Advanced Lectures*, (January 2001), 249–257. https://doi.org/10.1007/3-540-44673-7

FAO. (2017). FAO statistic, Retrieved from http://www.fao.org/statistics/en/

Fang, Y., Zhang, H., Mao, Q., & Li, Z. (2018). Land cover classification with GF-3 polarimetric synthetic aperture radar data by random forest classifier and fast super-pixel segmentation. *Sensors (Switzerland)*, *18*(7). https://doi.org/10.3390/s18072014

Ferrazzoli, P., Guerriero, L., & Schiavon, G. (2013). Experimental and Model Investigation on Radar Classification Capability, (April 1999). https://doi.org/10.1109/36.752214

Fu, B., Wang, Y., Campbell, A., Li, Y., Zhang, B., Yin, S., … Jin, X. (2017). Comparison of object-based and pixel-based Random Forest algorithm for wetland vegetation mapping using high spatial resolution GF-1 and SAR data. *Ecological Indicators*, *73*, 105–117. https://doi.org/10.1016/j.ecolind.2016.09.029

Fieuzal, R., Baup, F., Marais-Sicre, C., 2013. MonitoringWheat and Rapeseed by Using Synchronous Optical and Radar Satellite Data—FromTemporal Signatures to Crop Parameters Estimation.

Haas, J., & Ban, Y. (2014). Urban growth and environmental impacts in Jing-Jin-Ji, the Yangtze, River Delta, and the Pearl River Delta. *International Journal of Applied Earth Observation and Geoinformation*, *30*(1), 42–55. https://doi.org/10.1016/j.jag.2013.12.012

Hall, J. C., Sytsma, K. J., & Iltis, H. H. (2002). Phylogeny of Capparaceae and Brassicaceae based on chloroplast sequence data. *American Journal of Botany*, *89*(11), 1826–1842. https://doi.org/10.3732/ajb.89.11.1826

Ho, T. (1998). The Random Subspace Method for Constructing Decision Forests. *IEEE Transactions on Pattern Analysis and Machine Intelligence*, *20*(8), 832–844.

Hu, Q., Hua, W., Yin, Y., Zhang, X., Liu, L., Shi, J., … Wang, H. (2017). Rapeseed research and production in China. *Crop Journal*, *5*(2), 127–135. https://doi.org/10.1016/j.cj.2016.06.005

Huang, W., Luo, J., & Zhang, J. (2012). *Remote Sensing - Applications*. (Escalante Boris, Ed.). InTech. Retrieved from http://www.intechopen.com/books/remote-sensing-applications/crop-disease-and-pest-monitoring-by-remote- sensing

Hütt, C., & Waldhoff, G. (2018). Multi-data approach for crop classification using multitemporal, dual-polarimetric TerraSAR-X data, and official geodata. *European Journal of Remote Sensing*, *51*(1), 62–74. https://doi.org/10.1080/22797254.2017.1401909

Jamali, A., & Abdul Rahman, A. (2019). SENTINEL-1 IMAGE CLASSIFICATION for CITY EXTRACTION BASED on the SUPPORT VECTOR MACHINE and RANDOM FOREST ALGORITHMS. *International Archives of the Photogrammetry, Remote Sensing and Spatial Information Sciences - ISPRS Archives*, *42*(4/W16), 297–302. https://doi.org/10.5194/isprs-archives-XLII-4-W16-297-2019

Jamali, Ali. (2019). A fit-for-purpose algorithm for environmental monitoring based on maximum likelihood, support vector machine, and random forest. *International Archives of the Photogrammetry, Remote Sensing and Spatial Information Sciences - ISPRS Archives*, *42*(3/W7), 25–32. https://doi.org/10.5194/isprs-archives-XLII-3-W7-25-2019

Jiao, X., Kovacs, J. M., Shang, J., McNairn, H., Walters, D., Ma, B., & Geng, X. (2014). Object-oriented crop mapping and monitoring using multi-temporal polarimetric RADARSAT-2 data. *ISPRS Journal of Photogrammetry and Remote Sensing*, *96*, 38–46. https://doi.org/10.1016/j.isprsjprs.2014.06.014

Kavats, O., Khramov, D., Sergieieva, K., & Vasyliev, V. (2019). Monitoring harvesting by time series of Sentinel-1 SAR data. *Remote Sensing*, *11*(21), 1–16. https://doi.org/10.3390/rs11212496

Koschke, L., Fürst, C., Lorenz, M., Witt, A., Frank, S., & Makeschin, F. (2013). The integration of crop rotation and tillage practices in the assessment of ecosystem services provision at the regional scale. *Ecological Indicators*, *32*, 157–171. https://doi.org/10.1016/j.ecolind.2013.03.008

Krautgartner, Roswitha Golya, G., Rehder, L. E., Boshnakova, M., Dobrescu, M., Flach, B., Wilson, Jennifer Dimosthenis, Faniadis, Marta, G., & Bolla, S. (2019). *Oilseeds and Products Annual*. Retrieved from https://apps.fas.usda.gov/newgainapi/api/report/downloadreportbyfilename?filename=Oilseeds and Products Annual_Vienna_EU-28_3-28-2019.pdf

Lampropoulos, G., Li, Y., & Liu, T. (2015). Advancements in estimating crop growth stages using RADARSAT-2 and TerraSAR-X polarimetric data. In *International Archives of the Photogrammetry, Remote Sensing and Spatial Information Sciences - ISPRS Archives* (Vol. XL-7/W3, pp. 1227–1232). https://doi.org/10.5194/isprsarchives-XL-7-W3-1227-2015

Landis, J. R., & Koch, G. G. (1977). The measurement of observer agreement for categorical data. Biometrics, 33(1), 159–174. https://doi.org/10.2307/2529310

Li, H., Zhang, C., Zhang, S., & Atkinson, P. M. (2020). Crop classification from full-year fully-polarimetric L-band UAVSAR time-series using the Random Forest algorithm. *International Journal of Applied Earth Observation and Geoinformation*, *87*(May 2019), 102032. https://doi.org/10.1016/j.jag.2019.102032

Li, M., & Bijker, W. (2019). Vegetable classification in Indonesia using Dynamic Time Warping of Sentinel-1A dual polarization SAR time series. *International Journal of Applied Earth Observation and Geoinformation*, *78*(February), 268–280. https://doi.org/10.1016/j.jag.2019.01.009

Liu, D., & Xia, F. (2010). Assessing object-based classification: Advantages and limitations. *Remote Sensing Letters*, *1*(4), 187–194. https://doi.org/10.1080/01431161003743173

Liu, J., Zhu, W., Atzberger, C., Zhao, A., Pan, Y., & Huang, X. (2018). A Phenology-Based Method to Map Cropping Patterns under a Wheat-Maize Rotation Using Remotely Sensed Time-Series Data. *Remote Sensing*, *10*(8), 1203. https://doi.org/10.3390/rs10081203

Lu, D., & Weng, Q. (2007). A survey of image classification methods and techniques for improving classification performance. International Journal of Remote Sensing, 28(5), 823–870.

Macrì Pellizzeri, T. (2003). Classification of polarimetric SAR images of suburban areas using joint annealed segmentation and "H/A/α" polarimetric decomposition. *ISPRS Journal of Photogrammetry and Remote Sensing*, *58*(1–2), 55–70. https://doi.org/10.1016/S0924-2716(03)00017-0

Mcnairn H, Brisco B. 2004. The application of C-band polarimetric SAR for agriculture: A review. Canadian Journal of Remote Sensing, 30, 525–542

McNairn, H., Jiao, X., Pacheco, A., Sinha, A., Tan, W., & Li, Y. (2018). Estimating canola phenology using synthetic aperture radar. *Remote Sensing of Environment*, *219*, 196–205. https://doi.org/10.1016/j.rse.2018.10.012

Mcnairn, H., Shang, J., Jiao, X., & Champagne, C. (2009). The Contribution of ALOS PALSAR Multipolarization and Polarimetric Data to Crop Classification. *IEEE Transactions on Geoscience and Remote Sensing*, *47*(1), 3981–3992. https://doi.org/10.1109/TGRS.2009.2026052

Mercier, A., Betbeder, J., Baudry, J., Le Roux, V., Spicher, F., Lacoux, J., … Hubert-Moy, L. (2020). Evaluation of Sentinel-1 & 2 time series for predicting wheat and rapeseed phenological stages. *ISPRS Journal of Photogrammetry and Remote Sensing*, *163*(September 2019), 231–256. https://doi.org/10.1016/j.isprsjprs.2020.03.009

Millard, K., & Richardson, M. (2013). Wetland mapping with LiDAR derivatives, SAR polarimetric decompositions, and LiDAR–SAR fusion using a random forest classifier. Canadian Journal of Remote Sensing, 39(4), 290–307. https://doi.org/10.5589/m13-038

Myneni, R. B., Maggion, S., Iaquinta, J., Privette, J. L., Gobron, N., Pinty, B., … Williams, D. L. (1995). Optical remote sensing of vegetation: Modeling, caveats, and algorithms. *Remote Sensing of Environment*, *51*(1), 169–188. https://doi.org/10.1016/0034-4257(94)00073-V

Nagy, A., Fehér, J., & Tamás, J. (2018). Wheat and maize yield forecasting for the Tisza river catchment using MODIS NDVI time series and reported crop statistics. *Computers and Electronics in Agriculture*, *151*(March), 41–49. https://doi.org/10.1016/j.compag.2018.05.035

Richards, M.A. Introduction to Radar Systems. In Fundamentals of radar Signal Processing; Tata McGraw-Hill Education: New York City, NY, USA, 2005; pp. 45–47, ISBN 978-0071444743.

Saka, S., & Kusdiana, D. (2001). Biodiesel fuel from rapeseed oil as prepared in supercritical methanol. *Fuel*, *80*(2), 225–231. https://doi.org/10.1016/S0016-2361(00)00083-1

Shang, X., & Chisholm, L. A. (2014). Classification of Australian Native Forest Species Using Hyperspectral Remote Sensing and Machine-Learning Classification Algorithms. IEEE Journal of Selected Topics in Applied Earth Observations and Remote Sensing, 7(6), 2481–2489. https://doi.org/10.1109/JSTARS.2013.2282166

Song, P., Mansaray, L. R., Huang, J., & Huang, W. (2018). Mapping paddy rice agriculture over China using AMSR-E time series data. *ISPRS Journal of Photogrammetry and Remote Sensing*, *144*(March), 469–482. https://doi.org/10.1016/j.isprsjprs.2018.08.015

Stankiewicz, K. A. (2006). The Efficiency of Crop Recognition on ENVISAT ASAR Images in Two Growing Seasons, *44*(4), 806–814.

Stendardi, L., Karlsen, S., Niedrist, G., Gerdol, R., Zebisch, M., Rossi, M., & Notarnicola, C. (2018). Exploiting Time Series of Sentinel-1 and Sentinel-2 Imagery to Detect Meadow Phenology in Mountain Regions. *Remote Sensing*, *219*(5), 196–205. https://doi.org/10.3390/rs11050542

Sun, Y., Li, J., Liu, X., Ren, Z., Zhou, Z., & Duan, Y. (2020). Spatially explicit analysis of trade-offs and synergies among multiple ecosystem services in Shaanxi Valley basins. *Forests*, *11*(2), 1–21. https://doi.org/10.3390/f11020209

TAO, J. bin, WU, W. bin, ZHOU, Y., WANG, Y., & JIANG, Y. (2017). Mapping winter wheat using phenological feature of peak before winter on the North China Plain based on time-series MODIS data. *Journal of Integrative Agriculture*, *16*(2), 348–359. https://doi.org/10.1016/S2095-3119(15)61304-1

Tatsumi, K., Yamashiki, Y., Canales Torres, M. A., & Taipe, C. L. R. (2015). Crop classification of upland fields using Random forest of time-series Landsat 7 ETM+ data. *Computers and Electronics in Agriculture*, *115*, 171–179. https://doi.org/10.1016/j.compag.2015.05.001

Toan, T. Le, Laur, H., Mougin, E., & Lopes, A. (1989). Multitemporal and dual-polarization observations of agrcultural vegetation covers by X-band SAR images. *IEEE Transactions on Geoscience and Remote Sensing*, *27*(6), 709–718. https://doi.org/10.1109/TGRS.1989.1398243

Torres-Sánchez, J., Peña, J. M., de Castro, A. I., & López-Granados, F. (2014). Multi-temporal mapping of the vegetation fraction in early-season wheat fields using images from UAV. *Computers and Electronics in Agriculture*, *103*, 104–113. https://doi.org/10.1016/j.compag.2014.02.009

Vaudour, E., Carey, V. A., & Gilliot, J. M. (2010). Digital zoning of South African viticultural terroirs using bootstrapped decision trees on morphometric data and multitemporal SPOT images. *Remote Sensing of Environment*, *114*(12), 2940–2950. https://doi.org/10.1016/j.rse.2010.08.001

Veloso, A., Mermoz, S., Bouvet, A., Le Toan, T., Planells, M., Dejoux, J. F., & Ceschia, E. (2017). Understanding the temporal behavior of crops using Sentinel-1 and Sentinel-2-like data for agricultural applications. *Remote Sensing of Environment*, *199*, 415–426. https://doi.org/10.1016/j.rse.2017.07.015

Wang, C., Zhang, Z., Chen, Y., Tao, F., Zhang, J., & Zhang, W. (2018). Comparing different smoothing methods to detect double-cropping rice phenology based on LAI products–a case study in the Hunan province of China. *International Journal of Remote Sensing*, *39*(19), 6405–6428. https://doi.org/10.1080/01431161.2018.1460504

Wang, D., Fang, S., Yang, Z., Wang, L., Tang, W., Li, Y., & Tong, C. (2018). A Regional Mapping Method for Oilseed Rape Based on HSV Transformation and Spectral Features. *ISPRS International Journal of Geo-Information*, *7*(6), 224. https://doi.org/10.3390/ijgi7060224

Wang, S., Azzari, G., & Lobell, D. B. (2019a). Crop type mapping without field-level labels : Random forest transfer and unsupervised clustering techniques. *Remote Sensing of Environment*, *222*(November 2018), 303–317. https://doi.org/10.1016/j.rse.2018.12.026

Wang, S., Azzari, G., & Lobell, D. B. (2019b). Crop type mapping without field-level labels: Random forest transfer and unsupervised clustering techniques. *Remote Sensing of Environment*, *222*(January), 303–317. https://doi.org/10.1016/j.rse.2018.12.026

Wiseman, G., McNairn, H., Homayouni, S., Shang, J., 2014. RADARSAT-2 polarimetric SAR response to crop biomass for agricultural production monitoring. IEEE Journal of Selected Topics in Applied Earth Observations and Remote Sensing 7 (11), 4461–4471.

Woźniak, E., Waszkowska, E., Zimny, T., Sowa, S., & Twardowski, T. (2019). The Rapeseed Potential in Poland and Germany in the Context of Production, Legislation, and Intellectual Property Rights. *Frontiers in Plant Science*, *10*(November), 1–11. https://doi.org/10.3389/fpls.2019.01423

Wu, F., Wang, C., Zhang, H., Zhang, B., & Tang, Y. (2011a). Rice crop monitoring in South China with RADARSAT-2 quad-polarization SAR data. *IEEE Geoscience and Remote Sensing Letters*, *8*(2), 196–200. https://doi.org/10.1109/LGRS.2010.2055830

Wu, F., Wang, C., Zhang, H., Zhang, B., & Tang, Y. (2011b). Rice crop monitoring in South China with RADARSAT-2 quad-polarization SAR data. *IEEE Geoscience and Remote Sensing Letters*, *8*(2), 196–200. https://doi.org/10.1109/LGRS.2010.2055830

Xiao, R., Guo, D., Ali, A., Mi, S., Liu, T., Ren, C., … Zhang, Z. (2019). Accumulation, ecological-health risks assessment, and source apportionment of heavy metals in paddy soils: A case study in Hanzhong, Shaanxi, China. *Environmental Pollution*, *248*, 349–357. https://doi.org/10.1016/j.envpol.2019.02.045

Zafar, S., Li, Y. L., Li, N. N., Zhu, K. M., & Tan, X. L. (2019). Recent advances in enhancement of oil content in oilseed crops. *Journal of Biotechnology*, *301*(February), 35–44. https://doi.org/10.1016/j.jbiotec.2019.05.307

Zhang, M., & Lin, H. (2019). Object-based rice mapping using time-series and phenological data. *Advances in Space Research*, *63*(1), 190–202. https://doi.org/10.1016/j.asr.2018.09.018

Zhang, X., & He, Y. (2013). Rapid estimation of seed yield using hyperspectral images of oilseed rape leaves. *Industrial Crops and Products*, *42*(1), 416–420. https://doi.org/10.1016/j.indcrop.2012.06.021